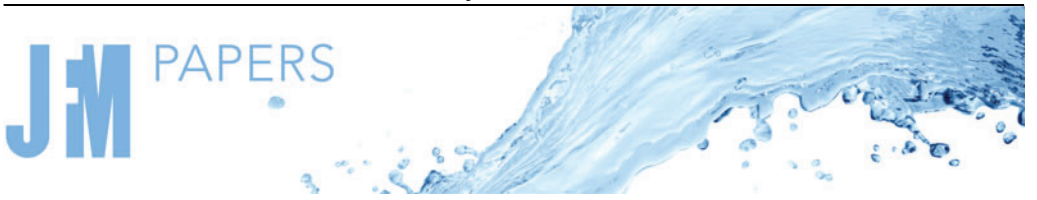
J. Fluid Mech. (2025), *vol*. 1003, A27, doi:10.1017/jfm.2024.1200



Small-scale interface dynamic modelling based on the geometric method of moments for a two-scale two-phase flow model with a disperse small scale

Arthur Loison[1],†, **Teddy Pichard**[1], **Samuel Kokh**[2] **and Marc Massot**[1]

[1]Institut Polytechnique de Paris, CMAP, CNRS, École polytechnique, Palaiseau 91120, France

[2]Service de Génie Logiciel pour la Simulation, Université Paris-Saclay, CEA, 91191 Gif-sur-Yvette, France

(Received 29 August 2023; revised 16 October 2024; accepted 4 December 2024)

In this contribution, we develop a versatile formalism to derive unified two-phase models describing both the separated and disperse regimes as introduced by Loison *et al.* (*Intl J. Multiphase Flow*, vol. 177, 2024, 104857). It relies on the stationary action principle and interface geometric variables. This contribution provides a novel method to derive small-scale models for the dynamics of the interface geometry. They are introduced here on a simplified case where all the scales and phases have the same velocity and that does not take into account large-scale capillary forces. The derivation tools yield a proper mathematical framework through hyperbolicity and signed entropy evolution. The formalism encompasses a hierarchy of small-scale reduced-order models based on a statistical description at a mesoscopic kinetic level and is naturally able to include the description of a disperse phase with polydispersity in size. This hierarchy includes both a cloud of spherical droplets and non-spherical droplets experiencing a dynamical behaviour through incompressible oscillations. The associated small-scale variables are moments of a number density function resulting from the geometric method of moments (GeoMOM). This method selects moments as small-scale geometric variables compatible with the structure and dynamics of the interface; they are defined independently of the flow topology and, therefore, this model allows the coupling of the two-scale flow with an inter-scale transfer. It is shown, in particular, that the resulting dynamics provides partial closures for the interface area density equation obtained from the averaging approach.

Key words: Hamiltonian theory, gas/liquid flow, aerosols/atomisation

† Email address for correspondence: arthur.loison@polytechnique.edu

© The Author(s), 2025. Published by Cambridge University Press

https://doi.org/10.1017/jfm.2024.1200 Published online by Cambridge University Press

1. Introduction

Two-phase flows encompass a wide range of physical phenomena, presenting dynamics involving a large spectrum of scales (Scardovelli & Zaleski 1999; Shinjo & Umemura 2010; Tomar *et al.* 2010; Dumouchel *et al.* 2015; Cordesse *et al.* 2020*b*; Estivalezes *et al.* 2022; Sakano *et al.* 2022). We identify, in particular, two different regimes based on the topology/geometry of the fluid interfaces (Ishii & Hibiki 1975): separated-phases flows, where the material interface is described at the bulk fluid scale (hereafter called large scale), and disperse flows, characterised by the presence of disperse phases within a carrier fluid, resulting in interfaces with significantly smaller scales (hereafter called small scale).

Simulating such flows is crucial for many industrial processes such as combustion chambers where liquid fuel is injected at high velocity and pressure forming a cloud of liquid droplets further away from the nozzle or nucleate boiling in nuclear reactors (Jamet *et al.* 2010; Providakis *et al.* 2012; Fiorina *et al.* 2016). Unfortunately, direct numerical simulation (DNS) capturing the smallest interfacial variations is currently limited to academic configurations and impractical in industrial contexts. We address these challenges through the development of new modelling approaches.

One such approach, known as sub-scale modelling, consists of modelling the sub-scale phenomena directly at the bulk scale. Various approaches have been proposed for both separated and disperse flow regimes, such as two-fluid systems of equations (Baer & Nunziato 1986; Raviart & Sainsaulieu 1995; Saurel, Chinnayya & Carmouze 2017). However, they often offer limited information about the interfacial structures and are only adapted to one of the two regimes. Several works aim at coupling both regimes (Devassy, Habchi & Daniel 2015; Le Touze *et al.* 2020) and sometimes include other modelling approaches such as Lagrangian models (Lebas *et al.* 2009). In the mixed regime zone, when the separated regime transitions to the disperse regime, the coupling processes involve very different descriptions, variables as well as a series of coupling parameters. They have to be tuned depending on the configuration of interest, which prevents the possibility of predictive simulations. The present work aims at providing a unified formalism that naturally degenerates towards separated and disperse flow models, and that can handle the mixed zone where both large and small scales are present.

This contribution takes advantage of a new versatile framework to derive unified two-scale two-phase models (Loison *et al.* 2024) based on Hamilton's stationary action principle (SAP) (Herivel 1955; Serrin 1959; Salmon 1983; Bedford 1985; Truskinovsky 1991; Gavrilyuk, Gouin & Perepechko 1998; Gouin & Gavrilyuk 1999; Gavrilyuk & Saurel 2002; Berdichevsky 2009; Drui *et al.* 2019; Cordesse *et al.* 2020*a*; Gouin 2020) and the second principle of thermodynamics. The originality of the approach relies on the models' ability to account for the presence of both separated and disperse regimes at the same time. This is made possible by considering an artificial mixture in which small-scale and large-scale interfaces coexist within the same physical domain. The length-scale threshold that separates the large-scale dynamics of the bulk phase from the dynamics of the small-scale depends on the physics and is not discussed in this work. By employing Hamilton's SAP and an evolution equation for the mathematical entropy of the model, we can obtain a dissipative system that captures the behaviour of this multiphase medium and provides a good mathematical framework to analyse such models.

The main contribution of this work lies in the ability to plug into this two-scale framework a hierarchy of small-scale models for the disperse flow regime coupled to the large scale via a liquid mass transfer. We notably extend the geometric method of moments (GeoMOM) of Essadki *et al.* (2019) which connects geometric description of the small-scale interfaces (Pope 1988; Drew 1990) with the statistics of a spray of droplets

https://doi.org/10.1017/jfm.2024.1200 Published online by Cambridge University Press

(Massot *et al.* 1998; Laurent & Massot 2001; Fox & Marchisio 2007; Massot 2007). We propose, in particular, a reduced-order moment model for the dynamics of the small-scale inclusions that degenerates toward an existing moment models for the disperse regime in the static minimal surface configuration of spherical polydisperse droplets (Kah *et al.* 2015; Essadki *et al.* 2018), but can also handle the dynamic case of incompressible oscillation of droplets at the kinetic level following O'Rourke & Amsden (1987) to model deformed inclusions. The key ingredient is the proper choice of variables, which are moments of this kinetic description, but can also be identified as surface-averaged geometric quantities related to the interface dynamics independently of the flow topology. By including an inter-scale transfer, this paves the way to the modelling of the mixed zone, where the shape of droplets and ligaments depart significantly from a spherical form.

Lastly, we demonstrate the compatibility of the obtained small-scale models with several existing models from the literature that describe the evolution of the interfacial area density in the flow. It offers a new way on selecting the adequate variables for interface dynamics description and reaches interesting closures, usually out of reach, for the interfacial area density equation.

The definition of the two-scale mixture and the derivation of its dynamics with Hamilton's SAP is recalled in § 2 following Loison *et al.* (2024). Then, the small-scale modelling of polydisperse sprays with GeoMOM is proposed in § 3. We pursue with an extension of the polydisperse model of spherical droplets into a spray of oscillating droplets in § 4. An inter-scale mass transfer coupling the resulting hierarchy of two-scale models is then defined in § 5. Finally, the dynamics of interface area density of these models is discussed and compared with models of the literature in § 6.

2. Two-scale two-phase model for both separated and disperse regimes

We model a mixture composed of large-scale liquid and gaseous phases in a separated regime and a small-scale liquid phase, the dynamics of which is characterised by a length scale yet to be determined. The regime of the small-scale phase is not prescribed here, but it is eventually described by a disperse regime model. This section recalls the two-scale model obtained in Loison *et al.* (2024) which proposes a framework to account for the presence of both large-scale and small-scale phases at the same location. The interested reader is referred to the discussions therein for more details.

2.1. *Two-scale modelling assumptions*

We propose successive sets of assumptions. First, regarding the fluid dynamics:

(a) all phases have the same mean velocity; (H1a)

(b) the small-scale velocity fluctuations and capillarity forces are modelled by a small-scale energy term; (H1b)

(c) the small-scale liquid phase is incompressible. (H1c)

Following hypotheses (H1a) and (H1b), we account for velocities that naturally appear at small scale (e.g. droplets' drag in the disperse regime) only through the advection of a local small-scale energy for the sake of clarity of the exposition of the new ideas of the paper. Potential extensions are discussed in the conclusion. The incompressibility of the small-scale is discussed in Appendix A to justify (H1c). It affects the physics at two levels. The first level pertains to sound propagation that is cancelled at the small scale. It is especially relevant in the disperse regime where no sound can propagate from one

https://doi.org/10.1017/jfm.2024.1200 Published online by Cambridge University Press

inclusion to another as underlined in Saurel *et al.* (2017). The second level is related to the volume occupation of the disperse phase and the evolution of its volume fraction.

Second, the following hypotheses are formulated solely for the sake of simplicity, but are not limiting for the models developed in the present work:

(a) each phase is isothermal with barotropic equations of state; (H2a)

(b) large-scale capillarity effects are not modelled; (H2b)

(c) no mass exchanges between the phases are taken into account; (H2c)

(d) body forces are neglected. (H2d)

Let us remark that (H1a) and (H2a) correspond to the thermal and kinematic equilibria as studied in Chanteperdrix, Villedieu & Vila (2002), Caro *et al.* (2005) and Drui *et al.* (2019). The effects neglected by (H2a), (H2b) and (H2c) have been studied, for instance, in Perigaud & Saurel (2005), Gaillard (2015), Schmidmayer *et al.* (2017), Cordesse (2020), Loison *et al.* (2024), Caro *et al.* (2005) and Pelanti (2022). The model can be extended to include these effects, but they are not necessary for the two-scale modelling framework at stake in this work. The particular modelling of mass transfer between the large scale and the small scale is not considered in this section but accounted in § 5.

We denote with the subscript $k = 1$ the liquid and $k = 2$ the gaseous phase. An additional superscript d identifies the small-scale liquid phase, where the letter d stands for 'droplets' or 'disperse' liquid phase. Following (H2a), each large-scale fluid $k = 1, 2$ is equipped with a barotropic equation of state of the form $\rho_k \mapsto e_k(\rho_k)$, where ρ_k and e_k are the density and the barotropic potential of the phase $k = 1, 2$. Denoting $(\cdot) \mapsto (\cdot)'$ the derivative with respect to the density, the pressure p_k of the large-scale phase $k = 1, 2$ is then defined by $p_k = \rho_k^2 e_k'(\rho_k)$. We assume that $p_k'(\rho_k) > 0$ so that the sound speed c_k associated with the phase $k = 1, 2$ is $c_k = \sqrt{p_k'(\rho_k)}$. With α_k the volume fraction of the phase $k = 1, 2, 1^d$, we consider a two-scale mixture such that it obeys the volume constraint

$$\alpha_1 + \alpha_2 + \alpha_1^d = 1, \tag{2.1}$$

and its density ρ is obtained from the effective phase densities $m_k := \alpha_k \rho_k$,

$$m_1 + m_2 + m_1^d = \rho. \tag{2.2}$$

Following Loison *et al.* (2024), we introduce the large-scale volume fractions defined by

$$\bar{\alpha}_k := \frac{\alpha_k}{1 - \alpha_1^d} \quad \text{for } k = 1, 2, \tag{2.3}$$

extending the usual definition at the large-scale perspective such that

$$\bar{\alpha}_1 + \bar{\alpha}_2 = 1. \tag{2.4}$$

We denote by Y_k the mass fraction such that the specific barotropic potential e of the two-phase material is defined by

$$e = Y_1 e_1(\rho_1) + Y_2 e_2(\rho_2) + Y_1^d e_1(\rho_1^d). \tag{2.5}$$

Under assumptions (H1a) and (H1b), there is a unique velocity $\boldsymbol{u}$ describing the mixture

$$\boldsymbol{u} := \boldsymbol{u}_1 = \boldsymbol{u}_2 = \boldsymbol{u}_1^d. \tag{2.6}$$

https://doi.org/10.1017/jfm.2024.1200 Published online by Cambridge University Press

Then, (H2*c*) provides the mass conservation of each phase

$$\partial_t m_k + \boldsymbol{\nabla} \cdot (m_k \boldsymbol{u}) = 0 \quad \text{for } k = 1, 2, 1^d. \tag{2.7}$$

Summing these equations provides the total mass conservation equation

$$\partial_t \rho + \boldsymbol{\nabla}_{\boldsymbol{x}} \cdot (\rho \boldsymbol{u}) = 0. \tag{2.8}$$

Denoting $D_t(\cdot) = \partial_t(\cdot) + \boldsymbol{u} \cdot \boldsymbol{\nabla}(\cdot)$ the material time derivative, the incompressibility of the small-scale liquid phase (H1*c*) reads

$$D_t \rho_1^d = 0. \tag{2.9}$$

Then liquid volume fraction of the small scale is conserved

$$\partial_t \alpha_1^d + \boldsymbol{\nabla} \cdot (\alpha_1^d \boldsymbol{u}) = 0. \tag{2.10}$$

The small-scale energy density accounting for both capillarity energy and kinetic energy of velocity fluctuations is advected at the mixture averaged velocity

$$D_t \zeta = 0. \tag{2.11}$$

2.2. *Conservative motion with Hamilton's SAP*

The equation of the two-scale fluid mixture's motion is derived similarly as Gavrilyuk & Gouin (1999) and Drui *et al.* (2019) by using Hamilton's SAP. We set the kinetic and potential energies of the phase k as

$$E_k^{kin} := \tfrac{1}{2} m_k \boldsymbol{u}^2, \quad E_k^{pot} := m_k e_k \left(\frac{m_k}{\alpha_k} \right), \tag{2.12a,b}$$

and the mixture kinetic and potential energies are $\sum_k E_k^{kin}$ and $\sum_k E_k^{pot}$. This enables the definition of the Lagrangian energy $\mathcal{L}_k = E_k^{kin} - E_k^{pot}$ of the phases $k = 1, 2$, $\mathcal{L}_1^d = E_1^{d,kin} - E_1^{d,pot} - m_1^d \zeta$ and a mixture Lagrangian energy $\mathcal{L} = \sum_k \mathcal{L}_k$. Capillarity energy at large scale is purposely not modelled for simplifying purposes (see (H2*b*)) and no particular flow regime is assumed for now at small scale. These effects are considered later in § 3, where we refine the small-scale model. Thereby, the Lagrangian associated with our system reads

$$\mathcal{L} = \mathcal{L}_1(\alpha_1, m_1, \boldsymbol{u}) + \mathcal{L}_2(\alpha_2, m_2, \boldsymbol{u}) + \mathcal{L}_1^d(m_1^d, \rho_1^d, \zeta, \boldsymbol{u}). \tag{2.13}$$

With mass conservation constraints, Hamilton's SAP leads to the following set of equations (see Appendix B for details)

$$\left.\begin{array}{c} \partial_t m_k + \boldsymbol{\nabla} \cdot (m_k \boldsymbol{u}) = 0, \quad k = 1, 2, 1^d, \\ \partial_t \alpha_1^d + \boldsymbol{\nabla} \cdot (\alpha_1^d \boldsymbol{u}) = 0, \\ \partial_t \zeta + \boldsymbol{u} \cdot \boldsymbol{\nabla} \zeta = 0, \\ \partial_t (\rho \boldsymbol{u}) + \boldsymbol{\nabla} \cdot (\rho \boldsymbol{u} \otimes \boldsymbol{u} + p \boldsymbol{I}) = 0, \end{array}\right\} \tag{2.14}$$

where $\boldsymbol{I}$ is the identity matrix, and p is the equilibrium pressure obtained for the mixture thermodynamic closure $p := p_1 = p_2$ given by the second line of (B16). This algebraic equation gives α_1 and p, respectively, as the solution and the value of the equilibrium for

https://doi.org/10.1017/jfm.2024.1200 Published online by Cambridge University Press

given values of m_1, m_2 and α_1^d. System (2.14) also admits a supplementary conservation equation

$$\partial_t \mathcal{H} + \boldsymbol{\nabla} \cdot ((\mathcal{H} + p)\boldsymbol{u}) = 0, \tag{2.15}$$

where the total energy $\mathcal{H} = \rho \|\boldsymbol{u}\|^2 - \mathcal{L}$ is a mathematical entropy (Godlewski & Raviart 1991) for (2.14). The mathematical entropy of the system is studied as the isothermal limit of the Euler–Fourier model in Serre (2010). It is shown to be convex and linked to the physical entropy of the mixture s with $\mathcal{H} = \rho(\varepsilon - Ts) + \frac{1}{2}\rho\|\boldsymbol{u}\|^2$ where $\varepsilon = e + Ts$ and T are the internal energy and the temperature of the mixture, respectively.

Remark that α_1 is not a variable of the set of conservation laws (2.14), but its effective dynamics for smooth solution can be written explicitly by applying the material time derivative to the algebraic equation $p_1(m_1/\alpha_1) = p_2(m_2/(1-\alpha_1-\alpha_1^d))$, and reads

$$D_t\alpha_1 = \Lambda \boldsymbol{\nabla} \cdot \boldsymbol{u} \quad \text{with } \Lambda = \alpha_1(1-\alpha_1)\frac{\rho_2 c_2^2 - \rho_1 c_1^2}{\alpha_1\rho_2 c_2^2 + (1-\alpha_1)\rho_1 c_1^2} + \alpha_1^d \frac{\alpha_1 \rho_2 c_2^2}{\alpha_1\rho_2 c_2^2 + (1-\alpha_1)\rho_1 c_1^2}. \tag{2.16}$$

Moreover, system (2.14) is shown hyperbolic with a mixture's velocity $c_W^d := c_W/(1-\alpha_1^d)$ where c_W is the Wood sound velocity such that $(c_W^2)^{-1} = \rho(\alpha_1/(\rho_1 c_1^2) + \alpha_2/(\rho_2 c_2^2))$. This extends, in particular, the three-equation model proposed by Chanteperdrix *et al.* (2002), which is recovered when $\alpha_1^d \to 0$.

Remark also that the small-scale specific energy ζ is chosen to be modelled here as a passively advected quantity. Therefore, it does not affect the dynamics of the two-scale mixture in absence of inter-scale mass transfer which is further modelled in § 5. The modelling of the effect of small-scale velocity fluctuations on large-scale dynamics, possibly via pressure contributions, is however out of the scope of this work. Because of this temporary passive role and for clarity purposes, this small-scale energy is removed from the modelling up to § 5.

2.3. *Dissipative dynamics*

Now that we have set the conservative structure of the model with Hamilton's SAP, we add dissipative processes to the model. We propose here to model both a pressure disequilibrium between the two large-scale phases as it is characteristic of two-phase flow models as in the model of Baer & Nunziato (1986) and fluid viscosity.

First, the pressure disequilibrium can encompass several physical phenomena with different timescales [e.g. bubbly flows (Drui *et al.* 2019) and stochastic thermodynamic relaxation (Perrier & Gutiérrez 2021)]. Let us mention that the limit of instantaneous relaxation can also be used to build a numerical scheme that solves the pressure equilibrium of (2.14) (Chanteperdrix *et al.* 2002).

In order to make this pressure relaxation a large-scale process that acts on each large-scale phase symmetrically, we define the large-scale volume fractions

$$\bar{\alpha}_k := \frac{\alpha_k}{1-\alpha_1^d} \quad \text{for } k = 1, 2, \tag{2.17}$$

such that for $\alpha_1^d < 1$,

$$\alpha_1 + \alpha_2 + \alpha_1^d = 1 \iff \bar{\alpha}_1 + \bar{\alpha}_2 = 1. \tag{2.18}$$

https://doi.org/10.1017/jfm.2024.1200 Published online by Cambridge University Press

Then, we relax the pressure equilibrium of (2.14) into

$$D_t\bar{\alpha}_1 = \frac{p_1 - p_2}{\epsilon}, \tag{2.19}$$

where $\epsilon > 0$ has the dimension of a dynamic viscosity. Since the pressure is no longer unique with this pressure relaxation, the momentum equation can be expressed as follows:

$$\partial_t(\rho\boldsymbol{u}) + \boldsymbol{\nabla}\cdot(\rho\boldsymbol{u}\otimes\boldsymbol{u} + \bar{p}\boldsymbol{I}) = 0, \tag{2.20}$$

where $\bar{p}$ is chosen to provide a signed dissipation of $\mathcal{H}$. Following Appendix B,

$$\begin{aligned}\varsigma &:= \partial_t\mathcal{H} + \boldsymbol{\nabla}\cdot((\mathcal{H}+\bar{p})\boldsymbol{u})\\ &= (\bar{p} - \alpha_1 p_1 - (\alpha_2 + \alpha_1^d)p_2)\boldsymbol{\nabla}\cdot\boldsymbol{u} - (p_1 - p_2)D_t\alpha_1\\ &= (\bar{p} - \bar{\alpha}_1 p_1 - \bar{\alpha}_2 p_2)\boldsymbol{\nabla}\cdot\boldsymbol{u} - \epsilon(1-\alpha_1^d)(D_t\bar{\alpha}_1)^2.\end{aligned} \tag{2.21}$$

Therefore, choosing $\bar{p} := \bar{\alpha}_1 p_1 + \bar{\alpha}_2 p_2$ gives a signed mathematical entropy production $\varsigma \leq 0$ and the relaxed model reads

$$\left.\begin{gathered}\partial_t m_k + \boldsymbol{\nabla}\cdot(m_k\boldsymbol{u}) = 0 \quad \text{for } k = 1, 2, 1^d,\\ \partial_t\alpha_1^d + \boldsymbol{\nabla}\cdot(\alpha_1^d\boldsymbol{u}) = 0,\\ \partial_t(\rho\boldsymbol{u}) + \boldsymbol{\nabla}\cdot(\rho\boldsymbol{u}\otimes\boldsymbol{u} + \bar{p}\boldsymbol{I}) = 0,\\ D_t\bar{\alpha}_1 = \epsilon^{-1}(p_1 - p_2).\end{gathered}\right\} \tag{2.22}$$

The model (2.22) is obtained for the specific dissipative process (2.19) that gives a relaxed model for (2.14). It is also shown hyperbolic with a mixture's velocity $c_F^d := c_F/(1-\alpha_1^d)$ where c_F is the frozen sound velocity such that $c_F^2 = Y_1c_1^2 + Y_2c_2^2$. The reader is referred to Loison *et al.* (2024) for a more thorough discussion on the pair of two-scale systems (2.14) and (2.22).

Second, the fluid viscosity in the context of a two-phase diffuse interface model with one velocity can be modelled with a Stokes source term on the momentum equation

$$\partial_t(\rho\boldsymbol{u}) + \boldsymbol{\nabla}\cdot(\rho\boldsymbol{u}\otimes\boldsymbol{u} + \bar{p}\boldsymbol{I}) = \boldsymbol{\nabla}\cdot\boldsymbol{T}_{stokes}, \tag{2.23}$$

where $\boldsymbol{T}_{stokes} := \mu(\boldsymbol{\nabla}\boldsymbol{u} + (\boldsymbol{\nabla}\boldsymbol{u})^{\mathrm{T}}) + \lambda(\boldsymbol{\nabla}\cdot\boldsymbol{u})\boldsymbol{I}$ is the viscous stress, μ the dynamic viscosity and λ the second viscosity with $\lambda + \frac{2}{3}\mu \geq 0$. After some calculations, this additional term modifies the mathematical entropy production (2.21) to yield

$$\begin{aligned}&\partial_t\mathcal{H} + \boldsymbol{\nabla}\cdot((\mathcal{H}+\bar{p})\boldsymbol{u} - \boldsymbol{T}_{stokes}\cdot\boldsymbol{u})\\ &\quad = -\epsilon(1-\alpha_1^d)(D_t\bar{\alpha}_1)^2 - \left(2\mu\left(\frac{\boldsymbol{\nabla}\boldsymbol{u} + (\boldsymbol{\nabla}\boldsymbol{u})^T}{2} - \frac{1}{3}(\boldsymbol{\nabla}\cdot\boldsymbol{u})\right)^2 + \left(\lambda + \frac{2}{3}\mu\right)(\boldsymbol{\nabla}\cdot\boldsymbol{u})^2\right).\end{aligned} \tag{2.24}$$

The right-hand side is negatively signed and thus provides a dissipative term to the dynamics.

Including these two viscosity terms, a dimensionless analysis of the dissipative system is proposed in Appendix C. In the remainder of this paper, such viscous terms are neglected for readability purposes, but their absence could also correspond to regimes with high fluid velocities.

We remark that other dissipative processes could have been considered, but are not modelled here, such as drag for two-velocity models (Saurel *et al.* 2017; Gavrilyuk 2020) or turbulent dissipation (Saurel, Gavrilyuk & Renaud 2003).

https://doi.org/10.1017/jfm.2024.1200 Published online by Cambridge University Press

3. Small-scale modelling consistent with polydisperse sprays of spherical droplets

We now follow two parallel goals to enrich the small-scale models of the previous section: (1) describing polydisperse sprays in the disperse regime, where the droplets are spherical, in their static minimal surface configuration; and (2) introducing geometric quantities which describe the small scale for any kind of interface in all flow regimes, thus proposing a limit model of a general interface dynamics at small scale. This modelling strategy has first been introduced for droplets in spherical shape in Essadki *et al.* (2016) and will be referred to in the present contribution as GeoMOM. This strategy relies on a kinetic modelling of the small scale as a population of droplets. The resulting model is consequently coherent in the disperse regime where the kinetic approach is valid. In the mixed regime, the physics validity of the kinetic-based model is limited, but it still remains interpretable since the chosen geometric variables are showed to be defined with both a large-scale modelling of the interface and the small-scale kinetic model.

3.1. *Kinetic-based model in the disperse regime*

We start the modelling of the spray by assuming that:

$$(a)\ \text{the small-scale phase is composed of spherical droplets;} \tag{H3a}$$

$$(b)\ \text{the droplets do not break nor coalesce.} \tag{H3b}$$

Indeed, (H1b) shows that only small velocity differences are locally allowed at the small scale, and droplets are then very close to a spherical shape. The droplets are then described by a static minimal surface, which remains spherical. The kinetic modelling of the disperse small scale relies on the number density function (NDF) f that counts the number of droplets within a small volume of the phase space around a point of the space–time domain. For generality purpose, we adopt a description for compressible inclusions whose sizes can change in time under either mass exchange or compressibility processes. Therefore, we consider the NDF $f(\boldsymbol{x}, t, \boldsymbol{v}, \hat{m})$ to be a distribution of velocities $\boldsymbol{v}$ and droplet masses $\hat{m}$ instead of a size parameter such as radius or surface. We also denote $f_{\boldsymbol{v},m}$ for compactness to underline the phase-space dependencies only. Then, the equation of evolution of the NDF expresses the conservation of the droplets in both the real and phase spaces (Williams 1958; Marchisio & Fox 2013) and reads

$$\partial_t f_{\boldsymbol{v},m} + \boldsymbol{\nabla}_{\boldsymbol{x}} \cdot (f_{\boldsymbol{v},m}\boldsymbol{v}) + \boldsymbol{\nabla}_{\boldsymbol{v}} \cdot (\boldsymbol{F}(\boldsymbol{v}, \hat{m}) f_{\boldsymbol{v},m}) + \partial_{\hat{m}}(R_m(\boldsymbol{v}, \hat{m}) f_{\boldsymbol{v},m}) = \Gamma, \tag{3.1}$$

where $\boldsymbol{F}$ and R_m are unclosed rates of change of the velocity and the mass corresponding to body forces and mass transfer, while $\Gamma = \Gamma_{bu} + \Gamma_{coal}$ accounts for source terms such as break-up and coalescence phenomena. Hypotheses (H3b) and (H2c) imply $\Gamma = 0$ and $R_m = 0$, respectively. Moreover, the distribution of velocities is out of the scope of this work as assumed by (H1a) (see Vié *et al.* 2013 for an Eulerian model coupling the effects of size and velocity distributions). Therefore, we discard the velocity dependency by considering $n_m = \int_{\boldsymbol{v}} f_{\boldsymbol{v},m}\, \mathrm{d}\boldsymbol{v}$, the mass-based NDF in the limit of a vanishing Stokes number $St \to 0$, i.e. when the inertial timescale of inclusions is negligible compared to the timescale of the flow. Following the works of Jabin (2002) and Massot (2007), the dynamics of n_m reads

$$\left.\begin{aligned} \partial_t n_m + \boldsymbol{\nabla}_{\boldsymbol{x}} \cdot (n_m \boldsymbol{u}) = 0, \\ \partial_t (n_m \boldsymbol{u}) + \boldsymbol{\nabla}_{\boldsymbol{x}} \cdot (n_m \boldsymbol{u} \otimes \boldsymbol{u}) = \boldsymbol{0}, \end{aligned}\right\} \tag{3.2}$$

where $\boldsymbol{u}$ is the unique velocity of every phase as defined by (2.6).

https://doi.org/10.1017/jfm.2024.1200 Published online by Cambridge University Press

3.2. *GeoMOM: definition and application to the incompressible spray*

GeoMOM aims at enriching the models (2.14)–(2.22) with quantities describing the geometry of the interface at the small scale. This method introduced in Essadki *et al.* (2016, 2018, 2019) is a reduced-order moment model for the polydisperse droplet distribution where the chosen moments are geometric quantities that can be defined for any flow regime and interface topology.

First, let us define those quantities. We consider a surface $\mathcal{S}$ defined by mapping a set $\mathcal{U} \subset \mathbb{R}^2$ onto $\mathcal{S} \subset \mathbb{R}^3$ such that we denote by $A(u, v)\,\mathrm{d}u\,\mathrm{d}v$ the infinitesimal surface element over $\mathcal{S}$. Then, the surface area and a surface-average operator are defined on $\mathcal{S}$ by

$$S := \int_{\mathcal{U}} A(u, v)\,\mathrm{d}u, \mathrm{d}v, \quad \langle\cdot\rangle := \frac{1}{S}\int_{\mathcal{U}} (\cdot)A(u, v)\,\mathrm{d}u\,\mathrm{d}v. \tag{3.3a,b}$$

Considering the surface of the droplets in the two-scale mixture as described in § 2, the sum of their areas defines the small-scale interface area density Σ. Thanks to (3.3), one can also define surface-average Gauss and mean curvatures $\Sigma\langle G\rangle$ and $\Sigma\langle H\rangle$ as in Drew (1983) and Pope (1988). We use here these quantities to enhance the description of the disperse small scale, but their definitions are *a priori* independent of the surface geometry (see an application of these geometric quantities to the interface resulting from for the collision of two spherical droplets in Appendix D). This property is particularly convenient as it indicates that the kinetic-based model can be interpreted as a limit case for the mixed regime, and we discuss in conclusion how it allows coupling of the interface geometry between scales.

Second, we reduce the complexity of the spray dynamics, modelled by the distribution n_m given in (3.2), by introducing a finite set of moments indexed by $\mathcal{I}$

$$M_i^m := \int_{\hat{m}} \hat{m}^i n_m\,\mathrm{d}\hat{m}, \quad i \in \mathcal{I} \text{ finite } \subset \mathbb{N}. \tag{3.4}$$

These scalars retain statistical information about the NDF and their dynamics can be obtained by integrating (3.2) against the corresponding monomials,

$$\partial_t M_i^m + \boldsymbol{\nabla}\cdot(M_i^m \boldsymbol{u}) = 0, \quad i \in \mathcal{I}. \tag{3.5}$$

The method of moments then gives a reduced-order model for the small-scale spray in comparison with (3.2). In general, the equations are unclosed, and a reconstruction of the NDF based on the selected moments must be provided. The selection of these moments is not obvious and is usually motivated on the basis of mathematical properties of the resulting moment model.

Finally, the specificity of GeoMOM consists in the selection of moments related to geometric quantities defined with (3.3) to construct a model interpretable even out of the disperse regime. For the spherical droplets described by n_m, the local Gauss and mean curvatures on the sphere are constant and equal to R^{-1} and R^{-2}, respectively, where $R = (3m/(4\pi\rho_1^d))^{1/3}$ is the radius of the sphere of density ρ_1^d and mass m. Therefore, considering a population of spherical droplets, we express the geometric quantities Σ,

https://doi.org/10.1017/jfm.2024.1200 Published online by Cambridge University Press

$\Sigma\langle G\rangle$ and $\Sigma\langle H\rangle$ as moments of the distribution n_m

$$\Sigma\langle G\rangle = \int_{\hat{m}} 4\pi n_m \,\mathrm{d}\hat{m} = 4\pi M_0^m, \tag{3.6a}$$

$$\Sigma\langle H\rangle = \int_{\hat{m}} 4\pi \left(\frac{3}{4\pi\rho_1}\right)^{1/3} \hat{m}^{1/3} n_m \,\mathrm{d}\hat{m} = 4\pi \left(\frac{3}{4\pi\rho_1^d}\right)^{1/3} M_{1/3}^m, \tag{3.6b}$$

$$\Sigma = \int_{\hat{m}} 4\pi \left(\frac{3}{4\pi\rho_1^d}\right)^{2/3} \hat{m}^{2/3} n_m \,\mathrm{d}\hat{m} = 4\pi \left(\frac{3}{4\pi\rho_1^d}\right)^{2/3} M_{2/3}^m. \tag{3.6c}$$

Remark the special role of $\Sigma\langle G\rangle$ proportional to the zeroth-order moment of n_m. This results from the Gauss–Bonnet theorem (Kreyszig 1991), which indicates a geometric invariant $S\tilde{G} = 4\pi$ for continuous deformations of the sphere, where $\widetilde{(\cdot)}$ denotes the surface average as (3.3) applied to a unique droplet. It is also shown in Essadki *et al.* (2019) that such an invariant enables to write the dynamics of geometric quantities Σ, $\Sigma\langle\cdot\rangle$ independently of the flow regime. Furthermore, the small-scale volume fraction is not surface-related in general, but in the specific case of spherical droplets, it is also linked to a moment of n_m with

$$\alpha_1^d = \int_{\hat{m}} \frac{1}{\rho_1^d} \hat{m} n_m \,\mathrm{d}\hat{m} = \frac{1}{\rho_1^d} M_1^m. \tag{3.7}$$

From (3.6) and (3.7), we select $\mathcal{I} = \{0, 1/3, 2/3, 1\}$ in (3.5) to obtain the dynamics of the geometric quantities

$$\left.\begin{array}{c} \partial_t(\Sigma\langle G\rangle) + \boldsymbol{\nabla}\cdot(\Sigma\langle G\rangle \boldsymbol{u}) = 0, \\ \partial_t((\rho_1^d)^{1/3}\Sigma\langle H\rangle) + \boldsymbol{\nabla}\cdot((\rho_1^d)^{1/3}\Sigma\langle H\rangle \boldsymbol{u}) = 0, \\ \partial_t((\rho_1^d)^{2/3}\Sigma) + \boldsymbol{\nabla}\cdot((\rho_1^d)^{2/3}\Sigma \boldsymbol{u}) = 0, \\ \partial_t m_1^d + \boldsymbol{\nabla}\cdot(m_1^d \boldsymbol{u}) = 0. \end{array}\right\} \tag{3.8}$$

Up to here, the model has been derived for compressible spherical inclusions. We focus back on the description of a spray of droplets by assuming the incompressibility of the small scale thanks to the constraint $D_t\rho_1^d = 0$. Then, the geometric variables are governed by

$$\left.\begin{array}{c} \partial_t(\Sigma\langle G\rangle) + \boldsymbol{\nabla}\cdot(\Sigma\langle G\rangle \boldsymbol{u}) = 0, \\ \partial_t(\Sigma\langle H\rangle) + \boldsymbol{\nabla}\cdot(\Sigma\langle H\rangle \boldsymbol{u}) = 0, \\ \partial_t\Sigma + \boldsymbol{\nabla}\cdot(\Sigma \boldsymbol{u}) = 0, \\ \partial_t\alpha_1^d + \boldsymbol{\nabla}\cdot(\alpha_1^d \boldsymbol{u}) = 0. \end{array}\right\} \tag{3.9}$$

System (3.9) corresponds to the system with surface-based moments of Essadki *et al.* (2018) when no evaporation nor condensation is accounted for. Indeed, when the droplets are incompressible, the mass-based NDF n_m relates to the surface-based NDF n_S defined by

$$n_S(\boldsymbol{x}, t, \hat{S}) := n_m(\boldsymbol{x}, t, \hat{m})\delta(\hat{m} - m(\hat{S})), \quad m(\hat{S}) = \rho_1^d \frac{\hat{S}}{3\sqrt{4\pi}}. \tag{3.10}$$

As ρ_1^d is a constant along the streamlines, there is no variation of surface area for the droplets and the dynamics is then driven by

$$\partial_t n_S + \boldsymbol{\nabla}_{\boldsymbol{x}}(n_S \boldsymbol{u}) = 0. \tag{3.11}$$

https://doi.org/10.1017/jfm.2024.1200 Published online by Cambridge University Press

Again, when the droplets have the same density, the geometric quantities are also expressed through the moments M_i^S of n_S,

$$\Sigma\langle G\rangle = 4\pi M_0^S, \quad \Sigma\langle H\rangle = \sqrt{4\pi}M_{1/2}^S, \quad \Sigma = M_1^S, \quad \alpha_1^d = \frac{1}{3\sqrt{4\pi}}M_{3/2}^S. \tag{3.12a–d}$$

The change of variables (3.10) only modifies the dimensions and orders of the moments. Consequently, the four initial half-integer moments can be recovered as in Essadki *et al.* (2018). In the following, we stick with the surface-based moments for better comparison with the work of Essadki *et al*. In the end, the relations (3.12) between moments and geometric quantities provide a reduced-order model of the small-scale disperse phase (see Appendix D for an illustration of the reduced-order modelling applied to droplets resulting from the collision of two spherical droplets).

3.3. *A two-scale model with a polydisperse small-scale model*

The two-scale models derived in § 2 thanks to Hamilton's SAP can now be enhanced by incorporating the new geometric quantities in the Lagrangian and specifying whether these parameters are constrained by new conservation laws. We add then a small-scale capillarity energy $\sigma\,\Sigma$ along with the conservation constraints given by (3.9). Let us introduce a new variable $z = \Sigma/m_1^d$, which is transported, that is, $D_t z = 0$. As the large-scale capillarity is neglected (H2*b*), the energies associated with the large scales of the flow are left unchanged whereas the small-scale Lagrangian $\mathcal{L}_1^d$ becomes

$$\mathcal{L}_1^d(m_1^d, \rho_1^d, z := \Sigma/m_1^d, \boldsymbol{u}) := \tfrac{1}{2}m_1^d|\boldsymbol{u}|^2 - m_1^d e_1(\rho_1^d) - \sigma m_1^d z. \tag{3.13}$$

Eventually, the system resulting from Hamilton's SAP (see details in Appendix E) together with the constraints (3.9) yields

$$\left.\begin{array}{c} \partial_t m_k + \boldsymbol{\nabla}\cdot(m_k\boldsymbol{u}) = 0, \quad k = 1, 2, 1^d, \\ \partial_t\alpha_1^d + \boldsymbol{\nabla}\cdot(\alpha_1^d\boldsymbol{u}) = 0, \\ \partial_t\Sigma + \boldsymbol{\nabla}\cdot(\Sigma\boldsymbol{u}) = 0, \\ \partial_t(\Sigma\langle G\rangle) + \boldsymbol{\nabla}\cdot(\Sigma\langle G\rangle\boldsymbol{u}) = 0, \\ \partial_t(\Sigma\langle H\rangle) + \boldsymbol{\nabla}\cdot(\Sigma\langle H\rangle\boldsymbol{u}) = 0, \\ \partial_t(\rho\boldsymbol{u}) + \boldsymbol{\nabla}\cdot(\rho\boldsymbol{u}\otimes\boldsymbol{u} + p\boldsymbol{I}) = 0, \end{array}\right\} \tag{3.14}$$

with $p := p_1 = p_2$. Let us remark that the new small-scale capillarity term in the Lagrangian does not alter momentum flux in this formulation compared to (2.14). Similarly to the previous models but with the updated definition of the Lagrangian $\mathcal{L}$, this model also admits a supplementary conservation equation

$$\partial_t\mathcal{H} + \boldsymbol{\nabla}\cdot((\mathcal{H}+p)\boldsymbol{u}) = 0, \quad \mathcal{H} = \sum_k m_k\|\boldsymbol{u}\|^2 - \mathcal{L}. \tag{3.15}$$

Both (3.14) and its relaxed version are hyperbolic with similar structure of eigenvalues and eigenvectors.

4. Polydisperse and vibrational spray small-scale model

In the previous model, no dynamics have been associated with the geometric variables as they represent a spray of spherical droplets, that is a static minimal surface. Here, we propose to enhance this model by associating a dynamics to the droplet geometry.

https://doi.org/10.1017/jfm.2024.1200 Published online by Cambridge University Press

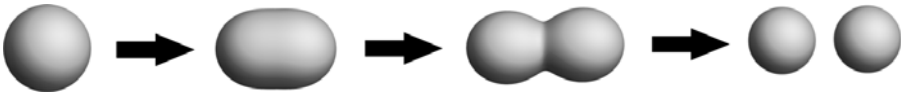


Figure 1. Sphere deformed with the second axisymmetric spherical harmonic and vibrational breakup modelled by a critical length for the smallest radius.

In the context of the small velocity differential given by (H1*b*), we add an oscillating motion to the droplets around their spherical shapes. Such a model is sufficiently simple to identify the associated energies while being a first step towards the modelling of break-up as proposed in O'Rourke & Amsden (1987) and Amsden, O'Rourke & Butler (1989) (see figure 1). Moreover, this model introduces with GeoMOM non-trivial dynamics for geometric quantities such as interface area density.

4.1. *Kinetic-based model in the disperse regime*

Let us model the spray of oscillating droplets by first discarding assumption (H3*a*) of spherical shapes, and rather assume:

(*a*) the droplets' internal flow is irrotational; (H4*a*)

(*b*) the amplitude of the interface deformation is small; (H4*b*)

(*c*) the deformed droplets are either randomly orientated or they all orientate to the same privileged direction; (H4*c*)

(*d*) the droplets' interface is deformed along the second axisymmetric spherical harmonic. (H4*d*)

The dynamics of a droplet satisfying (H4*a*) and (H4*b*) has been studied thoroughly (Rayleigh 1879; Prosperetti 1977; Plümacher *et al.* 2020). The choice of orientation (H4*c*) of the deformation depends on the physics, whether it is isotropic or not, and it is not discussed here. Denote by $\boldsymbol{r}$ the position of the droplet interface in spherical coordinates (r, θ, ϕ) and $(\boldsymbol{e}_r, \boldsymbol{e}_\theta, \boldsymbol{e}_\phi)$ the spherical orthonormalised basis. Following (H4*d*), we denote by $Y_2(\theta) = \sqrt{5}/(4\sqrt{\pi})(3\cos^2\theta - 1)$ the second axisymmetric spherical harmonic, and R_0 the radius of the non-deformed spherical droplet, such that the position can be written as

$$\boldsymbol{r} = (R_0 + x_2 Y_2)\boldsymbol{e}_r, \tag{4.1}$$

where x_2 denotes the amplitude of the deformation. The dynamics of this motion follows the harmonic oscillation

$$\ddot{x}_2 + \omega^2 x_2 = 0, \quad \omega^2 = 8\frac{\sigma}{\rho_1^d R_0^3} = \tilde{\omega}^2 S_0^{-3/2}, \tag{4.2}$$

where $\tilde{\omega}^2 = (8(4\pi)^{3/2}\sigma/\rho_1^d)$ is a constant along the streamlines. The dynamics of the droplets is then characterised by $(S_0, x_2, \dot{x}_2)$. For computational reasons, we introduce $\chi = (2/S_0)^{1/2}x_2$ which satisfies the same dynamics (4.2) as x_2. Assuming (H3*b*) and (H2*c*), the balance equation for the NDF n_ξ in the phase space $\hat{\boldsymbol{\xi}} = (\hat{S}_0, \hat{\chi}, \hat{\dot{\chi}})$ yields

$$\partial_t n_\xi + \boldsymbol{\nabla}_{\boldsymbol{x}} \cdot (n_\xi \boldsymbol{u}) + \partial_{\hat{\chi}}(R_\chi n_\xi) + \partial_{\hat{\dot{\chi}}}(R_{\dot{\chi}} n_\xi) = 0, \tag{4.3}$$

where R_χ and $R_{\dot{\chi}}$ are rates of change that remain to be closed. This model can be seen as the particular case satisfying (H1*a*)–(H2*c*)–(H3*b*)–(H2*a*) of the kinetic model considered

https://doi.org/10.1017/jfm.2024.1200 Published online by Cambridge University Press

by O'Rourke & Amsden (1987), Amsden *et al.* (1989). With the oscillator model (4.2), we close (4.3) by fixing $R_\chi = \hat{\dot{\chi}}$ and $R_{\hat{\dot{\chi}}} = -\tilde{\omega}^2 \hat{S}_0^{-3/2} \hat{\chi}$,

$$\partial_t n_\xi + \boldsymbol{\nabla}_{\boldsymbol{x}} \cdot (n_\xi \boldsymbol{u}) + \partial_{\hat{\chi}} (\hat{\dot{\chi}} n_\xi) + \partial_{\hat{\dot{\chi}}} (-\tilde{\omega}^2 \hat{S}_0^{-3/2} \hat{\chi} n_\xi) = 0. \tag{4.4}$$

4.2. *Modelling a spray of asynchronously oscillating droplets*

With the new PBE (4.4), GeoMOM leads to a non-trivial closure problem and the geometric quantities chosen in (3.6) and (3.7) cannot model an arbitrary distribution. With such a choice, we propose in this section to approximate the distribution with

$$n_\xi(\boldsymbol{x}, t, \hat{S}_0, \hat{\chi}, \hat{\dot{\chi}}) = n_{S_0}(\boldsymbol{x}, t, \hat{S}_0) \frac{1}{|\mathcal{E}(\hat{S}_0)|} \mathbb{1}_{\mathcal{E}(\hat{S}_0)}(\hat{\chi}, \hat{\dot{\chi}}), \tag{4.5}$$

where the amplitudes and their rates of change $(\hat{\chi}, \hat{\dot{\chi}})$ are uniformly distributed on a compact space $\mathcal{E} \subset \mathbb{R}^2$ of area $|\mathcal{E}(\hat{S}_0)|$ that allows a maximal energy for a given droplet size $\hat{S}_0$. This approximation of the NDF discards situations where droplets oscillate synchronously, and consequently a macroscopic oscillation motion of the spray.

4.2.1. *GeoMOM based on the classical surface-average operator*

We apply GeoMOM with the same surface-average operators $\langle\cdot\rangle$ and $\widetilde{(\cdot)}$ defined in § 3.2, and geometric quantities $\Sigma\langle G\rangle$, $\Sigma\langle H\rangle$, Σ, α_1^d. We establish then the relations between these geometric quantities and moments of the NDF in the context of a disperse regime,

$$\left.\begin{aligned} \Sigma\langle G\rangle = \int_{\hat{\boldsymbol{\xi}}} S\tilde{G} n_\xi \,\mathrm{d}\hat{\boldsymbol{\xi}}, \quad \Sigma\langle H\rangle = \int_{\hat{\boldsymbol{\xi}}} S\tilde{H} n_\xi \,\mathrm{d}\hat{\boldsymbol{\xi}}, \\ \Sigma = \int_{\hat{\boldsymbol{\xi}}} S n_\xi \,\mathrm{d}\hat{\boldsymbol{\xi}}, \quad \alpha_1^d = \int_{\hat{\boldsymbol{\xi}}} V n_\xi \,\mathrm{d}\hat{\boldsymbol{\xi}}. \end{aligned}\right\} \tag{4.6}$$

When the oscillations are small, the integrands are functions of $\hat{\boldsymbol{\xi}}$ (see Appendix F) and write

$$S\tilde{G} = 4\pi, \quad S\tilde{H} - S_0\tilde{H}_0 = \sqrt{4\pi} S_0^{1/2} \chi^2, \quad V = \frac{1}{3\sqrt{4\pi}} S_0^{3/2}, \quad S - S_0 = S_0 \chi^2, \tag{4.7a–d}$$

where $\tilde{H}_0 = \sqrt{4\pi} S_0^{-1/2}$ is the surface-averaged mean curvature when the droplet is a sphere, i.e. $\chi = 0$. We remark that $S\tilde{G}$ and α_1^d are constant despite the oscillation thanks to the Gauss–Bonnet theorem (Kreyszig 1991) and the incompressibility assumption. Finally, relations between geometric quantities and moments $M^\xi_{i,j,k} := \int_{\hat{\boldsymbol{\xi}}} \hat{S}^i \hat{\chi}^j \hat{\dot{\chi}}^k n_\xi \,\mathrm{d}\hat{\boldsymbol{\xi}}$ of n_ξ are obtained

$$\left.\begin{aligned} \Sigma\langle G\rangle = 4\pi M^\xi_{0,0,0}, \quad \Sigma\langle H\rangle = \sqrt{4\pi}(M^\xi_{1/2,0,0} + M^\xi_{1/2,2,0}), \\ \Sigma = M^\xi_{1,0,0} + M^\xi_{1,2,0}, \quad \alpha_1^d = \frac{1}{3\sqrt{4\pi}} M^\xi_{3/2,0,0}. \end{aligned}\right\} \tag{4.8}$$

These relations extend those of (3.12) with moments dedicated to the oscillatory dynamics. Such decomposition leads us to define and choose the following geometric quantities and

https://doi.org/10.1017/jfm.2024.1200 Published online by Cambridge University Press

moments for our model

$$\left.\begin{aligned} \Sigma\langle H\rangle_0 &:= \sqrt{4\pi}M^{\xi}_{1/2,0,0}, \quad \Delta\Sigma\langle H\rangle := \sqrt{4\pi}M^{\xi}_{1/2,2,0},\\ \Sigma_0 &:= M^{\xi}_{1,0,0}, \quad \Delta\Sigma := M^{\xi}_{1,2,0}, \end{aligned}\right\} \tag{4.9}$$

instead of just Σ and $\Sigma\langle H\rangle$ which can be reconstructed with (4.8). Integrating (4.4) against $(1, \hat{S}_0^{1/2}, \hat{S}_0, \hat{S}_0^{3/2}, \hat{S}_0^{1/2}\hat{\chi}^2, \hat{S}_0\hat{\chi}^2)$ provides

$$\left.\begin{aligned} \partial_t(\Sigma\langle G\rangle) + \nabla\cdot(\Sigma\langle G\rangle\boldsymbol{u}) &= 0,\\ \partial_t(\Sigma\langle H\rangle_0) + \nabla\cdot(\Sigma\langle H\rangle_0\boldsymbol{u}) &= 0,\\ \partial_t\Sigma_0 + \nabla\cdot(\Sigma_0\boldsymbol{u}) &= 0,\\ \partial_t\alpha_1^d + \nabla\cdot(\alpha_1^d\boldsymbol{u}) &= 0,\\ \partial_t(\Delta\Sigma\langle H\rangle) + \nabla\cdot(\Delta\Sigma\langle H\rangle\boldsymbol{u}) &= 2\sqrt{4\pi}M^{\xi}_{1/2,1,1},\\ \partial_t(\Delta\Sigma) + \nabla\cdot(\Delta\Sigma\boldsymbol{u}) &= 2M^{\xi}_{1,1,1}. \end{aligned}\right\} \tag{4.10}$$

We obtained that $\Sigma\langle G\rangle$, $\Sigma\langle H\rangle_0$, Σ_0 and α_1^d are conserved similarly as (3.9) with two additional equations for the oscillatory components $\Delta\Sigma\langle H\rangle$ and $\Delta\Sigma$.

4.2.2. *Energies of the spray*

In the context of two-scale modelling with Hamilton's SAP, we are specifically interested in defining the energies of the spray with the geometric quantities. For the oscillatory motion described by (4.2), the kinetic and potential energies of a droplet can be expressed as function of $\boldsymbol{\xi}$ (Rayleigh 1879, Appendix II)

$$E^{kin,1d} = \frac{1}{2}\frac{\rho_1^d}{4(4\pi)^{3/2}}S_0^{5/2}\dot{\chi}^2, \quad E^{pot,1d} = \sigma S = \sigma S_0 + \sigma S_0\chi^2. \tag{4.11a,b}$$

It is then straightforward to obtain the energies of the spray $E^{kin,d}$ and $E^{pot,d}$ from moments of n_ξ by integrating the expressions above,

$$E^{kin,d} = \frac{1}{2}\frac{\rho_1^d}{4(4\pi)^{3/2}}M^{\xi}_{5/2,0,2}, \quad E^{pot,d} = \sigma\,\Sigma = \sigma M^{\xi}_{1,0,0} + \sigma M^{\xi}_{1,2,0}. \tag{4.12a,b}$$

Remark that the moment $M^{\xi}_{5/2,0,2}$ is not linked to any of the selected geometric quantities of the model. We can find a closure for this moment using the approximation of n^{ξ} given in (4.5). It requires to provide a definition for $\mathcal{E}$ which is chosen following the break-up criterion of O'Rourke & Amsden (1987). Therefore, we authorise the droplets to oscillate with an energy lower than a fraction $c \in [0, 1]$ of the maximal energy E_{max} before break-up,

$$\mathcal{E}(\hat{S}_0) := \{(\hat{\chi}, \hat{\dot{\chi}}) \in \mathbb{R}^2 \text{ s.t. } E^{kin,1d}(\hat{S}_0, \hat{\chi}, \hat{\dot{\chi}}) + E^{pot,1d}(\hat{S}_0, \hat{\chi}, \hat{\dot{\chi}}) \leq cE_{max}(\hat{S}_0)\}. \tag{4.13}$$

The break-up energy $E_{max}(S_0)$ corresponds to a deformation up to an equatorial radius reaching half the value of the spherical radius

$$R_{eq} := \|\boldsymbol{r}(\pi/2)\| = \frac{R_0}{2}. \tag{4.14}$$

Then, the subset $\mathcal{E}$ boils down to $\mathcal{E} = \{\chi^2 + (\dot{\chi}/\omega)^2 \leq 2c/5\}$ whose area is $|\mathcal{E}| = \frac{2}{5}\pi\omega c$. We can now close the expression of $E^{kin,d}$, $E^{pot,d}$ in (4.11) and find the dynamics of the

https://doi.org/10.1017/jfm.2024.1200 Published online by Cambridge University Press

parameter c using (4.10) and the approximation of the NDF (4.5). It yields

$$E^{kin,d} = \tfrac{1}{10} c\sigma\,\Sigma_0, \quad E^{pot,d} = \sigma\,\Sigma_0 + \tfrac{1}{10} c\sigma\,\Sigma_0, \quad D_t c = 0. \tag{4.15a–c}$$

We remark that, as $(\chi\,,\,\dot{\chi})$ are uniformly distributed in $\mathcal{E}$, the mechanical energy is evenly distributed between kinetic and potential energies. Regarding the dynamics of c, the energy of the oscillation is advected along the streamline. Moreover, using the relation $\Delta\Sigma = M^{\xi}_{1,2,0}$, one can replace c by geometric quantities with $c = 10\Delta\Sigma/\Sigma_0$.

4.2.3. *Two-scale model with the small-scale spray model of asynchronous droplets*

Energies related to the small-scale oscillation are negatively signed in Hamilton's SAP as the kinetic energy is not a quadratic form of any kind of velocity. Indeed, the energy of the droplets is here considered as a whole energetic contribution without following their specific dynamics. Remark that the specific oscillatory energies for the small-scale are advected by the flow and then partly accounts for the velocity fluctuations introduced in § 2. While not being accounted here, the fluctuation energy term would be defined as the energy contribution of the velocity fluctuations which is not associated with droplets oscillations. We keep then the expression of the Lagrangian defined in (2.13), where we only modify the small-scale energies of $\mathcal{L}^d_1$ following

$$\mathcal{L}^d_1 := \frac{1}{2} m^d_1 \|\boldsymbol{u}\|^2 - m^d_1 e_1(\rho^d_1) - \sigma\,\Sigma_0 \left(1 + \frac{c}{5}\right). \tag{4.16}$$

The constraints are the same as in § 3 with the additional advection constraint $D_t c = 0$. The derivation of the two-scale mixture's dynamics with Hamilton's SAP is very similar to that of Appendix E and yields

$$\left.\begin{array}{c} \partial_t m_k + \boldsymbol{\nabla}\cdot(m_k\boldsymbol{u}) = 0, \quad k = 1, 2, 1^d, \\ \partial_t \alpha^d_1 + \boldsymbol{\nabla}\cdot(\alpha^d_1\boldsymbol{u}) = 0, \\ \partial_t \Sigma_0 + \boldsymbol{\nabla}\cdot(\Sigma_0\boldsymbol{u}) = 0, \\ \partial_t(\Delta\Sigma) + \boldsymbol{\nabla}\cdot(\Delta\Sigma\boldsymbol{u}) = 0, \\ \partial_t(\Sigma\langle G\rangle) + \boldsymbol{\nabla}\cdot(\Sigma\langle G\rangle\boldsymbol{u}) = 0, \\ \partial_t(\Sigma\langle H\rangle_0) + \boldsymbol{\nabla}\cdot(\Sigma\langle H\rangle_0\boldsymbol{u}) = 0, \\ \partial_t(\rho\boldsymbol{u}) + \boldsymbol{\nabla}\cdot(\rho\boldsymbol{u}\otimes\boldsymbol{u} + p\boldsymbol{I}) = 0, \end{array}\right\} \tag{4.17}$$

with $p := p_1 = p_2$, and the additional equation on total energy as a mathematical entropy for (4.17),

$$\partial_t\mathcal{H} + \boldsymbol{\nabla}\cdot((\mathcal{H} + p)\boldsymbol{u}) = 0, \quad \mathcal{H} = \sum_k m_k\|\boldsymbol{u}\|^2 - \mathcal{L}. \tag{4.18}$$

Now considering dissipation processes, we could also add the pressure relaxation as in the previous two-scale models. We propose here to focus on the dissipation associated to the small-scale oscillatory dynamics. Indeed, the oscillation motion eventually decreases and the associated energy dissipates into thermal energy or small-scale kinetic energy of the gas phase. Each of these last two energies are not modelled here, so the system loses this energy, and we only consider the following source term R_c on the dynamics of c,

$$D_t c = R_c. \tag{4.19}$$

The mathematical entropy production may be written as

$$\varsigma := \partial_t\mathcal{H} + \boldsymbol{\nabla}\cdot((\mathcal{H} + p)\boldsymbol{u}) = -(\partial_c\mathcal{L})R_c. \tag{4.20}$$

As $\partial_c\mathcal{L} = -\sigma\,\Sigma_0/5$, we choose $R_c = -c/\tau$ to sign the mathematical entropy production $\varsigma \leq 0$ and model the dissipation with an exponential decrease of characteristic time $\tau > 0$.

https://doi.org/10.1017/jfm.2024.1200 Published online by Cambridge University Press

The final system reads

$$\left.\begin{array}{c}\partial_t m_k + \boldsymbol{\nabla}\cdot(m_k\boldsymbol{u}) = 0, \quad k = 1, 2, 1^d,\\ \partial_t \alpha_1^d + \boldsymbol{\nabla}\cdot(\alpha_1^d\boldsymbol{u}) = 0,\\ \partial_t \Sigma_0 + \boldsymbol{\nabla}\cdot(\Sigma_0\boldsymbol{u}) = 0,\\ \partial_t(\Delta\Sigma) + \boldsymbol{\nabla}\cdot(\Delta\Sigma\boldsymbol{u}) = -\tau^{-1}\Delta\Sigma,\\ \partial_t(\Sigma\langle G\rangle) + \boldsymbol{\nabla}\cdot(\Sigma\langle G\rangle\boldsymbol{u}) = 0,\\ \partial_t(\Sigma\langle H\rangle_0) + \boldsymbol{\nabla}\cdot(\Sigma\langle H\rangle_0\boldsymbol{u}) = 0,\\ \partial_t(\rho\boldsymbol{u}) + \boldsymbol{\nabla}\cdot(\rho\boldsymbol{u}\otimes\boldsymbol{u} + p\boldsymbol{I}) = 0,\end{array}\right\} \tag{4.21}$$

with $p := p_1 = p_2$. One can see that the component of the interface area density modelling the droplets' dynamics have now its own dynamics with an additional source term that makes it dissipate over time.

4.3. *Modelling a spray of synchronously oscillating droplets*

With the choice of geometric quantities of the previous section, the moments are not suited to obtain a macroscopic oscillation of the spray. Therefore, we introduce now new geometric quantities with GeoMOM based on another surface-average operator, and the following NDF approximation

$$n_\xi(\hat{S}_0, \hat{\chi}, \hat{\dot{\chi}}) = \sum_i n_i \delta(\hat{S}_0 - (S_0)_i)\delta(\hat{\chi} - \chi_i)\delta(\hat{\dot{\chi}} - \dot{\chi}_i). \tag{4.22}$$

This corresponds to several populations of droplets which share the same size and oscillate synchronously.

4.3.1. *GeoMOM based on an oriented surface-average operator*

Similarly to § 3.2, we consider a surface $\mathcal{S}$ and its mapping $\mathcal{U} \subset \mathbb{R}^2$ onto $\mathcal{S} \subset \mathbb{R}^3$ such that $A(u, v)\,\mathrm{d}u\,\mathrm{d}v$ is the infinitesimal surface element over $\mathcal{S}$. We decompose the surface local area into two contributions, one related to a preferred direction $\boldsymbol{N}$ given by the large-scale dynamics as suggested by (H4*c*). In this sense, we decompose this infinitesimal surface element $A(u, v)\,\mathrm{d}u\,\mathrm{d}v$ using its definition using tangential vectors $\boldsymbol{e}_u$ and $\boldsymbol{e}_v$

$$A = \|\boldsymbol{e}_u \times \boldsymbol{e}_v\|, \quad A_\parallel = |(\boldsymbol{e}_u \times \boldsymbol{e}_v)\cdot\boldsymbol{N}|, \quad A_\perp = A - A_\parallel. \tag{4.23a–c}$$

From them, we decompose the surface into parallel and perpendicular components $S_\parallel$ and $S_\perp$ such that

$$S = \int_{\mathcal{U}} A(u, v)\,\mathrm{d}u\,\mathrm{d}v = \int_{\mathcal{U}} A_\parallel(u, v)\,\mathrm{d}u\,\mathrm{d}v + \int_{\mathcal{U}} A_\perp(u, v)\,\mathrm{d}u\,\mathrm{d}v = S_\parallel + S_\perp. \tag{4.24}$$

We also define new surface-average operators similarly to (3.3)

$$\langle\cdot\rangle_\parallel := \frac{1}{S_\parallel}\int_{\mathcal{U}} (\cdot)A_\parallel(u, v)\,\mathrm{d}u\,\mathrm{d}v, \quad \langle\cdot\rangle_\perp := \frac{1}{S_\perp}\int_{\mathcal{U}} (\cdot)A_\perp(u, v)\,\mathrm{d}u\,\mathrm{d}v, \tag{4.25a,b}$$

and the surface-average operators $\widetilde{(\cdot)}^\parallel$, $\widetilde{(\cdot)}^\perp$ for one closed inclusion. Considering now the oscillatory motion (4.2), we have the following dynamics for the geometric quantities of

https://doi.org/10.1017/jfm.2024.1200 Published online by Cambridge University Press

one droplet (see details in Appendix F)

$$\left.\begin{aligned} S_\parallel &= \frac{1}{2}S_0 - \frac{1}{\sqrt{4\pi}}\sqrt{\frac{5\pi}{2}}S_0\chi, \quad S_\parallel\tilde{H}^\parallel = \frac{1}{2}\sqrt{4\pi}\sqrt{S_0} - \frac{1}{2}\sqrt{\frac{5\pi}{2}}\sqrt{S_0}\chi, \\ S_\perp &= \frac{1}{2}S_0 + \frac{1}{\sqrt{4\pi}}\sqrt{\frac{5\pi}{2}}S_0\chi, \quad S_\perp\tilde{H}^\perp = \frac{1}{2}\sqrt{4\pi}\sqrt{S_0} + \frac{1}{2}\sqrt{\frac{5\pi}{2}}\sqrt{S_0}\chi. \end{aligned}\right\} \tag{4.26}$$

Defining the oriented interface area densities $\Sigma_\perp$ and $\Sigma_\parallel$ within the mixture, we remark that $\Sigma = \Sigma_\perp + \Sigma_\parallel$ and $\Sigma\langle\cdot\rangle = \Sigma_\perp\langle\cdot\rangle_\perp + \Sigma_\parallel\langle\cdot\rangle_\parallel$. Integrating (4.26) against n_ξ provides

$$\left.\begin{aligned} \Sigma_\parallel &= \frac{1}{2}M^\xi_{1,0,0} - \frac{1}{\sqrt{4\pi}}\sqrt{\frac{5\pi}{2}}M^\xi_{1,1,0}, \quad (\Sigma\langle H\rangle)_\parallel = \frac{1}{2}\sqrt{4\pi}M^\xi_{1/2,0,0} - \frac{1}{2}\sqrt{\frac{5\pi}{2}}M^\xi_{1/2,1,0}, \\ \Sigma_\perp &= \frac{1}{2}M^\xi_{1,0,0} + \frac{1}{\sqrt{4\pi}}\sqrt{\frac{5\pi}{2}}M^\xi_{1,1,0}, \quad (\Sigma\langle H\rangle)_\perp = \frac{1}{2}\sqrt{4\pi}M^\xi_{1/2,0,0} + \frac{1}{2}\sqrt{\frac{5\pi}{2}}M^\xi_{1/2,1,0}. \end{aligned}\right\} \tag{4.27}$$

Remark that both the parallel and perpendicular geometric variables represent the same information for the spray as they are related to the same moments of the NDF. Consequently, we here retain the perpendicular components only, and we extract the part dedicated to the dynamics by defining

$$\left.\begin{aligned} \Sigma_{\perp,0} &:= \tfrac{1}{2}M^\xi_{1,0,0}, \quad (\Delta\Sigma_\perp) := \frac{1}{\sqrt{4\pi}}\sqrt{\frac{5\pi}{2}}M^\xi_{1,1,0}, \\ (\Sigma\langle H\rangle)_{\perp,0} &:= \tfrac{1}{2}\sqrt{4\pi}M^\xi_{1/2,0,0}, \quad (\Delta\Sigma\langle H\rangle)_\perp := \frac{1}{2}\sqrt{\frac{5\pi}{2}}M^\xi_{1/2,1,0}. \end{aligned}\right\} \tag{4.28}$$

We intentionally factored some indexes in the two last geometric quantities to lighten the notations. This splitting allows us to retain more information on the NDF in our model by including two moments rather than the sum of two moments. We know from (4.10) that $\Sigma_{\perp,0}$ and $(\Sigma\langle H\rangle)_{\perp,0}$ are conserved, while we integrate (4.4) to obtain the dynamics of the two other geometric quantities

$$\left.\begin{aligned} \partial_t(\Delta\Sigma_\perp) + \nabla\cdot((\Delta\Sigma_\perp)\boldsymbol{u}) &= \frac{1}{\sqrt{4\pi}}\sqrt{\frac{5\pi}{2}}M^\xi_{1,0,1}, \\ \partial_t(\Delta\Sigma\langle H\rangle)_\perp + \nabla\cdot((\Delta\Sigma\langle H\rangle)_\perp\boldsymbol{u}) &= \frac{1}{2}\sqrt{\frac{5\pi}{2}}M^\xi_{1/2,0,1}. \end{aligned}\right\} \tag{4.29}$$

With the moments considered up to now, we cannot model a macroscopic oscillatory spray as we lack some information regarding the distribution of $\hat{\chi}$ in our model. We propose then to add two new geometric quantities that correspond to the unclosed moments of (4.29)

$$\left.\begin{aligned} (\Delta_t\Sigma_\perp) &:= \Sigma_\perp\left\langle\frac{\partial_t A_\perp}{A_\perp}\right\rangle_\perp = \frac{1}{\sqrt{4\pi}}\sqrt{\frac{5\pi}{2}}M^\xi_{1,0,1}, \\ (\Delta_t\Sigma\langle H\rangle)_\perp &:= \Sigma_\perp\left\langle\partial_t H + H\frac{\partial_t A_\perp}{A_\perp}\right\rangle_\perp = \frac{1}{2}\sqrt{\frac{5\pi}{2}}M^\xi_{1/2,0,1}. \end{aligned}\right\} \tag{4.30}$$

The above definitions with the oriented surface-average operators show that these quantities are also well-defined regardless of the flow regime. Finally, we consider the following eight geometric quantities to describe the spray of oscillating droplets: α_1^d, $\Sigma_{\perp,0}$, $(\Delta\Sigma_\perp)$, $(\Delta_t\Sigma_\perp)$, $(\Sigma\langle H\rangle)_{\perp,0}$, $(\Delta\Sigma\langle H\rangle)_\perp$, $(\Delta_t\Sigma\langle H\rangle)_\perp$ and $\Sigma\langle G\rangle$.

https://doi.org/10.1017/jfm.2024.1200 Published online by Cambridge University Press

4.3.2. *Amplitude-based closure*

With the eight moments given by the eight corresponding geometric quantities, we propose to look for a two-point quadrature which corresponds to two populations of droplets as defined in (4.22),

$$n_\xi(\hat{S}_0, \hat{\chi}, \hat{\dot{\chi}}) = \sum_{i=1,2} n_i \delta(\hat{S}_0 - (S_0)_i)\delta(\hat{\chi} - \chi_i)\delta(\hat{\dot{\chi}} - \dot{\chi}_i), \tag{4.31}$$

where n_i are the weights or numbers of droplets that share the same abscissas χ_i and $\dot{\chi}_i$. The quadrature above admits a unique solution (excluding symmetry) under some realisability conditions that ensure that $\Sigma\langle G\rangle$, $(\Sigma\langle H\rangle)_{\perp,0}$, $\Sigma_{\perp,0}$ and α_1^d are positive with additional geometric constraints (see Appendix G). Remark that n_i and $(S_0)_i$ depend only on $\Sigma\langle G\rangle$, $(\Sigma\langle H\rangle)_{\perp,0}$, $\Sigma_{\perp,0}$, α_1^d and, for $(i,j) \in \{(1,2),(2,1)\}$,

$$\left.\begin{aligned} \chi_i &= \sqrt{\frac{2}{5\pi}}\frac{\sqrt{4\pi}(\Delta\Sigma_\perp) - 2\sqrt{(S_0)_j}(\Delta\Sigma\langle H\rangle)_\perp}{n_i((S_0)_i - \sqrt{(S_0)_i(S_0)_j})}, \\ \dot{\chi}_i &= \sqrt{\frac{2}{5\pi}}\frac{\sqrt{4\pi}(\Delta_t\Sigma_\perp) - 2\sqrt{(S_0)_j}(\Delta_t\Sigma\langle H\rangle)_\perp}{n_i((S_0)_i - \sqrt{(S_0)_i(S_0)_j})}. \end{aligned}\right\} \tag{4.32}$$

We easily obtain that α_1^d, $\Sigma\langle G\rangle$, $(\Sigma\langle H\rangle)_{\perp,0}$ and $\Sigma_{\perp,0}$ are conserved such that, together with (4.29), it implies

$$\partial_t n_i + \nabla\cdot(n_i\boldsymbol{u}) = 0, \quad D_t(S_0)_i = 0, \quad D_t\chi_i = \dot{\chi}_i, \quad i = 1,2. \tag{4.33}$$

This dynamics is expected as the two populations of oscillating droplets are advected by the flow at velocity $\boldsymbol{u}$.

4.3.3. *Two-scale model with the small-scale spray model of synchronous droplets*

Denote $\nu := \rho_1^d/(4(4\pi)^{3/2})$ and $\gamma := 2\sigma$ such the kinetic and potential energies of the spray of oscillating droplets given in (4.11) can be written

$$E^{kin,d} = \tfrac{1}{2}\nu M^\xi_{5/2,0,2}, \quad E^{pot,d} = \sigma M^\xi_{1,0,0} + \tfrac{1}{2}\gamma M^\xi_{1,2,0}, \tag{4.34a,b}$$

and $\tilde{\omega}^2 = \gamma/\nu$. The closure (4.31) then yields

$$E^{kin,d} = \sum_{i=1,2}\frac{1}{2}\nu n_i (S_0)_i^{5/2}\dot{\chi}_i^2, \quad E^{pot,d} = \sum_{i=1,2}\sigma n_i (S_0)_i + \frac{1}{2}\gamma n_i (S_0)_i \chi_i^2. \tag{4.35a,b}$$

We extend the two-scale Lagrangian (2.13) by adding the energies above to account for the small-scale oscillation

$$\begin{aligned} \mathcal{L} = {} & \mathcal{L}_1(\alpha_1, m_1, \boldsymbol{u}) + \mathcal{L}_2(\alpha_2, m_2, \boldsymbol{u}) + \mathcal{L}_1^d(m_1^d, \rho_1^d, \boldsymbol{u}) \\ & + \mathcal{L}_1^{vib}(n_1, (S_0)_1, \chi_1, \dot{\chi}_1) + \mathcal{L}_2^{vib}(n_2, (S_0)_2, \chi_2, \dot{\chi}_1), \end{aligned} \tag{4.36}$$

where $\mathcal{L}_i^{vib}$ is defined using vibrating energies of (4.34)

$$\mathcal{L}_i^{vib} = \tfrac{1}{2}\nu n_i (S_0)_i^{5/2}\dot{\chi}_i^2 - \sigma n_i (S_0)_i - \tfrac{1}{2}\gamma n_i (S_0)_i \chi_i^2. \tag{4.37}$$

Recall that the kinetic energy is here positively signed as it is a quadratic form of $\dot{\chi}_1$ and $\dot{\chi}_2$ with their associated momentum equations after Hamilton's SAP. We also remark

https://doi.org/10.1017/jfm.2024.1200 Published online by Cambridge University Press

that similarly to the asynchronous case, a similar remark as that stated in § 4.2.3 holds regarding the modelling of small-scale energy fluctuations. We provided an expression using the quadrature's abscissas rather than the geometric quantities for computational convenience, but the dynamics of the geometric quantities is equivalently obtained using the quadrature expression of Appendix G. In addition to α_1, the quantities χ_1 and χ_2 are also free variables which results in the following system with two additional momentum equations for each population of droplets of same size in the spray (see Appendix H):

$$\left.\begin{array}{c}\partial_t m_k + \boldsymbol{\nabla}\cdot(m_k\boldsymbol{u}) = 0, \quad k = 1, 2, 1^d,\\ \partial_t n_i + \boldsymbol{\nabla}\cdot(n_i\boldsymbol{u}) = 0, \quad i = 1, 2,\\ \partial_t (n_i(S_0)_i) + \boldsymbol{\nabla}\cdot(n_i(S_0)_i\boldsymbol{u}) = 0, \quad i = 1, 2,\\ \partial_t (n_i\dot{\chi}_i) + \boldsymbol{\nabla}\cdot(n_i\dot{\chi}_i\boldsymbol{u}) = -\omega_i^2 n_i\chi_i, \quad i = 1, 2,\\ \partial_t (n_i\chi_i) + \boldsymbol{\nabla}\cdot(n_i\chi_i\boldsymbol{u}) = n_i\dot{\chi}_i, \quad i = 1, 2,\\ \partial_t(\rho\boldsymbol{u}) + \boldsymbol{\nabla}\cdot(\rho\boldsymbol{u}\otimes\boldsymbol{u} + p) = 0,\end{array}\right\} \tag{4.38}$$

with $p := p_1 = p_2$ and $\omega_i^2 = \tilde{\omega}^2 (S_0)_i^{-3/2}$. Combining the equations at the fifth and sixth lines of the system above, one can recognise the equations of harmonic oscillators advected along the streamlines

$$D_t(D_t\chi_i) + \omega_i^2\chi_i = 0, \quad i = 1, 2. \tag{4.39}$$

Similarly to the previous models, this system admits an additional conservation equation on the total energy $\mathcal{H}$ defined hereafter

$$\partial_t\mathcal{H} + \boldsymbol{\nabla}\cdot((\mathcal{H} + p)\boldsymbol{u}) = 0, \quad \mathcal{H} = \sum_{k=1,2,1^d}\frac{1}{2}m_k|\boldsymbol{u}|^2 + \sum_{i=1,2}\frac{1}{2}\nu n_i(S_0)_i^{5/2}\dot{\chi}_i^2 - \mathcal{L}. \tag{4.40}$$

Once again, we could consider a pressure relaxation model, but we would like to focus again on the dissipation associated to the oscillation process, and we introduce source terms R_{χ_i} in the new momentum equations

$$\partial_t(n_i\dot{\chi}_i) + \boldsymbol{\nabla}\cdot(n_i\dot{\chi}_i\boldsymbol{u}) = -\omega_i^2 n_i\chi_i + R_{\chi_i}, \quad i = 1, 2. \tag{4.41}$$

This source term provides the following mathematical entropy production:

$$\varsigma := \partial_t\mathcal{H} + \boldsymbol{\nabla}\cdot((\mathcal{H} + p)\boldsymbol{u}) = \sum_{i=1,2}\nu(S_0)_i^{5/2}R_{\chi_i}D_t\chi_i. \tag{4.42}$$

As the closure (4.31) groups droplets by size, we can now model the first-order size-dependent damping term of the viscous droplet in a light carrier phase (Prosperetti 1977; Plümacher *et al.* 2020). Then, we expect each population of oscillators to be damped following

$$D_t(D_t(\chi_i)) + \omega_i^2\chi_i = -\beta_i D_t\chi_i \iff D_t\dot{\chi}_i + \omega_i^2\chi_i = -\beta_i\dot{\chi}_i, \tag{4.43}$$

with $\beta_i = 4\pi\nu_{vis}/(S_0)_i > 0$ with ν_{vis} the liquid kinematic viscosity. One can then choose $R_{\chi_i} = -n_i\beta_i\dot{\chi}_i$ and recover both the above dissipation process for both populations of

https://doi.org/10.1017/jfm.2024.1200 Published online by Cambridge University Press

droplets and a signed production of mathematical entropy

$$\varsigma = -\beta_1 n_1 \nu (S_0)_1^{5/2} \dot{\chi}_1^2 - \beta_2 n_2 \nu (S_0)_2^{5/2} \dot{\chi}_2^2 \leq 0. \tag{4.44}$$

This leads to the following dissipative model:

$$\left.\begin{array}{c} \partial_t m_k + \boldsymbol{\nabla} \cdot (m_k \boldsymbol{u}) = 0, \quad k = 1, 2, 1^d, \\ \partial_t n_i + \boldsymbol{\nabla} \cdot (n_i \boldsymbol{u}) = 0, \quad i = 1, 2, \\ \partial_t (n_i (S_0)_i) + \boldsymbol{\nabla} \cdot (n_i (S_0)_i \boldsymbol{u}) = 0, \quad i = 1, 2, \\ \partial_t (n_i \dot{\chi}_i) + \boldsymbol{\nabla} \cdot (n_i \dot{\chi}_i \boldsymbol{u}) = -\omega_i^2 n_i \chi_i - \beta_i n_i \dot{\chi}_i, \quad i = 1, 2, \\ \partial_t (n_i \chi_i) + \boldsymbol{\nabla} \cdot (n_i \chi_i \boldsymbol{u}) = n_i \dot{\chi}_i, \quad i = 1, 2, \\ \partial_t (\rho \boldsymbol{u}) + \boldsymbol{\nabla} \cdot (\rho \boldsymbol{u} \otimes \boldsymbol{u} + p \boldsymbol{I}) = 0, \end{array}\right\} \tag{4.45}$$

with $p := p_1 = p_2$. This model shows a macroscopic synchronous oscillation through the two momentum equations on $\dot{\chi}_1$ and $\dot{\chi}_2$ and includes a physics-based dissipation rate. The system is here written using the weights and abscissas, but it can also be written using the geometric quantities of the model.

5. Inter-scale coupling transfer for the two-scale model with asynchronously oscillating droplets

In this section, we provide an example of inter-scale transfer that takes advantage of the enhanced description of the small scale with more geometric quantities and demonstrates the modelling capabilities of the primary break-up. We consider the two-scale model (4.17) where the small-scale droplets are oscillating asynchronously. Considering a process that mimics a liquid atomisation, we would like to add now an inter-scale transfer from large-scale liquid phase to the small-scale phase via source terms. Such a transfer requires a small amount of energy as the interface area density increases when droplets are created. Thus, we introduce back the small-scale energy ζ defined in § 2, which now only contains the small-scale energy of velocity fluctuations not related to the oscillatory motion of the droplets. Let us then modify (4.17) to obtain

$$\left.\begin{array}{c} \partial_t m_1 + \boldsymbol{\nabla} \cdot (m_1 \boldsymbol{u}) = R_{m_1}, \\ \partial_t m_1^d + \boldsymbol{\nabla} \cdot (m_1^d \boldsymbol{u}) = R_{m_1^d}, \\ \partial_t m_2 + \boldsymbol{\nabla} \cdot (m_2 \boldsymbol{u}) = 0, \\ \partial_t \alpha_1^d + \boldsymbol{\nabla} \cdot (\alpha_1^d \boldsymbol{u}) = R_{\alpha_1^d}, \\ \partial_t \Sigma_0 + \boldsymbol{\nabla} \cdot (\Sigma_0 \boldsymbol{u}) = R_{\Sigma_0}, \\ \partial_t (\Delta \Sigma) + \boldsymbol{\nabla} \cdot (\Delta \Sigma \boldsymbol{u}) = R_{\Delta \Sigma_0}, \\ \partial_t (\Sigma \langle G \rangle) + \boldsymbol{\nabla} \cdot (\Sigma \langle G \rangle \boldsymbol{u}) = R_{\Sigma \langle G \rangle}, \\ \partial_t (\Sigma \langle H \rangle_0) + \boldsymbol{\nabla} \cdot (\Sigma \langle H \rangle_0 \boldsymbol{u}) = R_{\Sigma \langle H \rangle_0}, \\ \partial_t (\rho \boldsymbol{u}) + \boldsymbol{\nabla} \cdot (\rho \boldsymbol{u} \otimes \boldsymbol{u} + p \boldsymbol{I}) = \boldsymbol{0}, \\ \partial_t \bar{\alpha}_1 + \boldsymbol{u} \cdot \boldsymbol{\nabla} \bar{\alpha}_1 = R_{\bar{\alpha}_1}, \\ \partial_t \zeta + \boldsymbol{u} \cdot \boldsymbol{\nabla} \zeta = R_\zeta, \end{array}\right\} \tag{5.1}$$

where R_X are the source terms of the equation on quantities $X \in \{m_1, m_1^d, \alpha_1^d, \Sigma_0, \Delta\Sigma, \Sigma\langle G \rangle, \Sigma\langle H \rangle_0, \bar{\alpha}_1, \zeta\}$. Remark that the choice of source terms differs from Loison *et al.* (2024) as no source term is set here on the momentum equations. In both cases, the goal is to give access to another source of energy. The source terms chosen keeps the Galilean invariance on the model, even though the numerical effect of a non-Galilean invariant source term was limited.

https://doi.org/10.1017/jfm.2024.1200 Published online by Cambridge University Press

Moreover, we also introduce a source term in the underlying PBE (4.4) that now reads

$$\partial_t n_\xi + \boldsymbol{\nabla}_{\boldsymbol{x}} \cdot (n_\xi \boldsymbol{u}) + \partial_{\hat{\chi}}(\dot{\hat{\chi}} n_\xi) + \partial_{\hat{\chi}}(-\tilde{\omega}^2 \hat{S}_0^{-3/2} \hat{\chi} n_\xi) = R_\xi(\widehat{S_0}, \hat{\chi}, \dot{\hat{\chi}}). \tag{5.2}$$

Note that the additional source term is not a collisional operator for coalescence or break-up but a coupling term with the large-scale model.

We can now identify constraints between source terms, first with the conservation of the liquid mass and the incompressibility which immediately gives

$$R_{m_1^d} = -R_{m_1}, \quad R_{\alpha_1^d} = -\frac{R_{m_1}}{\rho_1^d}. \tag{5.3a,b}$$

The source terms for geometric quantities related to the surface S_0 are derived according to the relations between moments and geometric quantities (4.8) and (4.9), it yields

$$\left.\begin{aligned} R_{\Sigma_0} = -\frac{S_{0,avg}}{m_{avg}} R_{m_1}, \quad R_{\Sigma\langle H\rangle_0} = -\frac{(S\tilde{H})_{0,avg}}{m_{avg}} R_{m_1}, \\ R_{\Sigma\langle G\rangle} = -\frac{4\pi}{m_{avg}} R_{m_1}, \quad R_{\alpha_1^d} = -\frac{R_{m_1}}{\rho_1^d}, \end{aligned}\right\} \tag{5.4}$$

where $S_{0,avg}$, $(S\tilde{H})_{0,avg}$ and m_{avg} are unclosed parameters. The source term $R_{\Delta\Sigma}$ can be decomposed in two contributions: a creation term arising from the mass transfer $R_{\Delta\Sigma,m}$ and a viscous damping $R_{\Delta\Sigma,v}$ as in system (4.21). As $\Delta\Sigma = 4\pi M_{1,2,0}$, the creation source term then reads

$$R_{\Delta\Sigma,m} = \int_\xi \widetilde{S_0} \tilde{\chi}^2 R_\xi(\widehat{S_0}, \hat{\chi}, \dot{\hat{\chi}}). \tag{5.5}$$

Let us then assume that

(a) the droplets are created at a fraction q of their maximal amplitude. (H5)

Given the definitions of § 4, that $\chi_{max}(S_0) = 2/\sqrt{5}$, such that the assumption translates as

$$R_{\Delta\Sigma,m} = \frac{4}{5} q^2 R_{\Sigma_0} = -\frac{4}{5} q^2 \frac{S_{0,avg}}{m_{avg}} R_{m_1}. \tag{5.6}$$

The source terms $R_{\tilde{\alpha}_1}$ $R_{\Delta\Sigma,v}$ R_{m_1} and $\boldsymbol{R_u}$ are left unconstrained for now. Now, the mathematical entropy dissipation rate ς associated with the energy $\mathcal{H}$ defined in (4.18) gives

$$\begin{aligned} \varsigma = &-(1-\alpha_1^d)(p_1 - p_2) R_{\tilde{\alpha}_1} + 2\sigma R_{\Delta\Sigma,v} \\ &- \left(e_1(\rho_1^d) + \frac{\bar{p}}{\rho_1^d} - \left(e_1(\rho_1) + \frac{p_1}{\rho_1} \right) + \sigma \left(1 + \frac{8}{5} q^2 \right) \left(\frac{S_{avg}}{m_{avg}} \right) \right) R_{m_1} + R_\zeta. \end{aligned} \tag{5.7}$$

We sign the two first terms, the pressure relaxation and the viscous damping of the oscillation, respectively, with

$$R_{\tilde{\alpha}_1} = -\frac{1}{\mu}(p_1 - p_2), \quad R_{\Delta\Sigma,v} = -\tau^{-1} \Delta\Sigma, \tag{5.8a,b}$$

https://doi.org/10.1017/jfm.2024.1200 Published online by Cambridge University Press

and $\mu, \tau > 0$ a dynamic viscosity and a damping timescale. The non-positivity of ς is then enforced by choosing

$$\left.\begin{aligned} R_{m_1} &= R_{m_{1,1}}(1 - \mathbb{1}_{C_1 \cap C_2}) + R_{m_{1,2}} \mathbb{1}_{C_1 \cap C_2}, \\ R_\zeta &= R_{m_{1,2}} \left(e_1^d + \frac{\bar{p}}{\rho_1^d} + \sigma \left(1 + \frac{8}{5} q^2\right) \frac{S_{avg}}{m_{avg}} - e_1 - \frac{p_1}{\rho_1} \right), \end{aligned}\right\} \tag{5.9}$$

with unclosed parameters $R_{m_{1,1}} < 0$ and $R_{m_{1,2}} < 0$ and both a thermodynamic disequilibrium condition and a small-scale energy availability condition

$$C_1 : \left(e_1^d + \frac{\bar{p}}{\rho_1^d} + \sigma \left(1 + \frac{8}{5} q^2\right) \frac{S_{avg}}{m_{avg}} > e_1 + \frac{p_1}{\rho_1} \right), \tag{5.10}$$

$$C_2 : \zeta > 0. \tag{5.11}$$

Because of the incompressibility of the small scale and its oscillatory motion, a small contribution of the small-scale energy density is sometimes needed to bridge the small thermodynamic disequilibrium (5.10) between the two liquid phases. In these conditions, for such inter-scale transfer to happen, one needs some small-scale energy density available (5.11), i.e. kinetic energy due to velocity fluctuations.

With its handful of unclosed parameters $S_{0,avg}$, $(S\tilde{H})_{0,avg}$, m_{avg}, q, τ, $R_{m_{1,1}}$ and $R_{m_{1,2}}$, this model allows a further modelling of the mechanism of the primary breakup. Such parameters can then be related to dimensionless number via heuristics to mimic experimental observation as can be found in Pilch & Erdman (1987). For instance, one can either create static inclusions by setting $q = 0$ or deformed inclusion on the verge of breaking up a second time by choosing $q = 1$. This initial deformation influences the dynamics of the inclusions right after the break-up. Depending on the oscillation pulsation, the damping timescale and additional source terms such as velocity drag, the initial deformation can either lead to a secondary break-up or not. Furthermore, the choice of parameters $S_{0,avg}$, $(S\tilde{H})_{0,avg}$ and m_{avg} influences the distribution in sizes of the resulting small-scale droplets. The determination of such relation is not, however, proposed in this work and is left for further study.

We remark that all the previous models provide peculiar interface area density dynamics which are specifically discussed in the next section.

6. Dynamics of the small-scale interface area density

To perceive the importance of the choice of variables and modelling choices made in the previous sections, in this last section we investigate their effect on the closure of the evolution equation for the interface area density. Such an equation is usually obtained from an averaging process and, whereas several terms are classically identified, their closure is most of the time out of reach except in very simplified configurations. We show how the proper choice of variables for both the static minimal surface spherical case, but also the dynamical case, allows a clear-cut strategy to close this important evolution equation and rethink the set of variables we should use for a unified model.

6.1. *Geometry of the disperse regime through the classical averaging approach*

First, the time evolution of the geometry for a generic two-phase flow is derived with an averaging process (Drew & Passman 1999; Lhuillier 2004; Morel 2015). This approach

https://doi.org/10.1017/jfm.2024.1200 Published online by Cambridge University Press

relies on the kinematics of the interface where the phases $k = 1, 2$ are located using a phase indicator function $\boldsymbol{X}_k$ and the interface is identified through its derivative $\boldsymbol{\nabla X}_k$ in the sense of generalised function. Denoting by $\boldsymbol{u}_I$ the interface velocity, the kinematics of the interface reads

$$\partial_t \boldsymbol{X}_k + \boldsymbol{u}_I \cdot \boldsymbol{\nabla X}_k = 0. \tag{6.1}$$

The ensemble-average operator $\langle\cdot\rangle_E$ is introduced such that the volume fraction and the interface area density are defined by $\alpha_k = \langle \boldsymbol{X}\rangle_E$ and $\Sigma = \langle\delta_I\rangle_E$ where $\delta_I = -\boldsymbol{n}\boldsymbol{\nabla X}_k$ is the interface generalised function. Then, the evolution of the interface area density is derived in Lhuillier (2004) as the trace of the interface tensor $\delta_I \boldsymbol{n}\otimes\boldsymbol{n}$. It eventually yields

$$\left.\begin{array}{c} \partial_t \alpha + \langle \boldsymbol{u}_I \cdot \boldsymbol{\nabla X}\rangle_E = 0, \\ \partial_t \Sigma + \boldsymbol{\nabla}\cdot\langle\delta_I \boldsymbol{u}_I\rangle_E = \langle \boldsymbol{I} - \boldsymbol{n}\otimes\boldsymbol{n} : \boldsymbol{\nabla} \boldsymbol{u}_I \delta_I\rangle_E. \end{array}\right\} \tag{6.2}$$

Such an averaging approach is compatible with the kinetic-based small-scale models of this work in the statistical sense. Similarly, the characteristics (size, oscillation amplitude, etc.) are following the probabilistic law given by the NDF. Focusing on the small-scale disperse regime while assuming (H1*a*), we have $\alpha = \alpha_1^d$, and we decompose $\boldsymbol{u}_I = \boldsymbol{u} + v_n\boldsymbol{n}$. Moreover, the symmetry of either spherical inclusions (H3*a*) or oscillation motion (H4*d*) gives $\langle v_n\boldsymbol{n}\delta_I\rangle_E = 0$. The averaged equations then become

$$\left.\begin{array}{c} D_t\alpha_1^d = -\langle v_n\boldsymbol{n}\cdot\boldsymbol{\nabla X}\rangle_E, \\ \partial_t\Sigma + \boldsymbol{\nabla}\cdot(\Sigma\boldsymbol{u}) = \dfrac{2}{3}\Sigma\boldsymbol{\nabla}\cdot\boldsymbol{u} - \langle\boldsymbol{q} : \boldsymbol{\nabla}\boldsymbol{u}\rangle_E + \dfrac{2}{3}\langle\boldsymbol{\nabla}\cdot(v_n\boldsymbol{n})\delta_I\rangle_E - \langle\boldsymbol{q}:\boldsymbol{\nabla}(v_n\boldsymbol{n})\rangle_E, \end{array}\right\} \tag{6.3}$$

where $\boldsymbol{q} = \langle(\boldsymbol{n}\otimes\boldsymbol{n} - \boldsymbol{I}/3)\delta_I\rangle_E$ is the anisotropic tensor. In this last equation, one can identify the different contributions to the interface area density evolution (from left to right of the right-hand side): the large-scale isotropic and anisotropic terms, the small-scale isotropic and anisotropic terms.

6.2. *Comparison with the small-scale models*

From the different small-scale models in this work, as well as proper choice of variables, we show that the interface area density equation of evolution can be thoroughly closed. We compare it with the unclosed kinematic set of equations (6.3) and identify the various contributions. The question of the choice of fundamental variables to describe the dynamics of the interface is eventually discussed.

6.2.1. *Spray of compressible spherical inclusions*

Before considering an incompressible small scale dedicated to the description of droplets, we focus on the case of compressible inclusions such as bubbles, which has been partially treated in § 3. We recast the unclosed dynamics for Σ obtained in (3.8) into

$$\partial_t\Sigma + \boldsymbol{\nabla}\cdot(\Sigma\boldsymbol{u}) = \frac{2}{3}\Sigma\boldsymbol{\nabla}\cdot\boldsymbol{u} + \frac{2}{3}\Sigma\frac{D_t\alpha_1^d}{\alpha_1^d}. \tag{6.4}$$

Even though the previous equation is unclosed as the dynamics of α_1^d is not specified, one can still identify the isotropic contribution of the large scale of (6.3). As we

https://doi.org/10.1017/jfm.2024.1200 Published online by Cambridge University Press

consider spherical shapes, $\boldsymbol{q} = \boldsymbol{0}$ and there are no anisotropic contributions. Therefore, the small-scale isotropic term is

$$\langle \boldsymbol{\nabla} \cdot (v_n \boldsymbol{n}) \delta_I \rangle_E = \Sigma \frac{D_t \alpha_1^d}{\alpha_1^d}. \tag{6.5}$$

A closed model is thus obtained with the dynamics of α_1^d as in the next case dealing with incompressible inclusions.

6.2.2. *Spray of incompressible spherical droplets*
The incompressible case has been treated in § 3 after assuming $D_t \rho_1^d = 0$. We have then the following conservation equations:

$$\left.\begin{aligned} \partial_t \alpha_1^d + \boldsymbol{\nabla} \cdot (\alpha_1^d \boldsymbol{u}) = 0, \\ \partial_t \Sigma + \boldsymbol{\nabla} \cdot (\Sigma \boldsymbol{u}) = 0. \end{aligned}\right\} \tag{6.6}$$

The anisotropic tensor $\boldsymbol{q}$ is still nil and provides trivial anisotropic closures, while the isotropic closures read

$$\langle v_n \boldsymbol{n} \cdot \boldsymbol{\nabla} \boldsymbol{X} \rangle_E = \alpha_1^d \boldsymbol{\nabla} \cdot \boldsymbol{u}, \quad \langle \boldsymbol{\nabla} \cdot (v_n \boldsymbol{n}) \delta_I \rangle_E = -\Sigma \boldsymbol{\nabla} \cdot \boldsymbol{u}. \tag{6.7a,b}$$

This shows that the small-scale isotropic contributions balance the large-scale ones to maintain the incompressibility of the small scale.

6.2.3. *Two-scale model with the small-scale spray model of asynchronous droplets*
This case has been treated in §§ 4.2 and 5, where the oscillatory dynamics of the incompressible droplets is formulated in a decomposed form of the small-scale interface area density following $\Sigma = \Sigma_0 + \Delta\Sigma$. Considering the case with inter-scale mass-transfer, this results in the following set of equations:

$$\left.\begin{aligned} \partial_t \alpha_1^d + \boldsymbol{\nabla} \cdot (\alpha_1^d \boldsymbol{u}) = 0, \\ \partial_t \Sigma + \boldsymbol{\nabla} \cdot (\Sigma \boldsymbol{u}) = -\frac{\Delta\Sigma}{\tau} - \left(\frac{S_{0,avg}}{m_{avg}} + \frac{4}{5} q^2 \frac{S_{0,avg}}{m_{avg}} \right) R_{m_1}. \end{aligned}\right\} \tag{6.8}$$

Following the assumption (H4*c*) made on the orientation of the oscillating droplets, one can consider the right-hand side term as either isotropic or anisotropic

$$\left.\begin{aligned} \langle v_n \boldsymbol{n} \cdot \boldsymbol{\nabla} \boldsymbol{X} \rangle_E = \alpha_1^d \boldsymbol{\nabla} \cdot \boldsymbol{u}, \\ \langle \boldsymbol{q} : \boldsymbol{\nabla} \boldsymbol{u} \rangle_E = 0, \\ \frac{2}{3} \langle \boldsymbol{\nabla} \cdot (v_n \boldsymbol{n}) \delta_I \rangle_E - \langle \boldsymbol{q} : \boldsymbol{\nabla} (v_n \boldsymbol{n}) \rangle_E = -\frac{2}{3} \Sigma \boldsymbol{\nabla} \cdot \boldsymbol{u} - \frac{\Delta\Sigma}{\tau} - \left(\frac{S_{0,avg}}{m_{avg}} + \frac{4}{5} q^2 \frac{S_{0,avg}}{m_{avg}} \right) R_{m_1}. \end{aligned}\right\} \tag{6.9}$$

The excess of interface area density $\Delta\Sigma$ results from the balance between the inter-scale creation term and the exponentially dissipative decreasing. It proposes an additional perspective to the balance between coalescence and break-up as can be found in Vallet & Borghi (1999) and Anez *et al.* (2019). This last phenomenon cannot be recovered here as we have not introduced any turbulence model for the small scale. This is the subject of a current work in progress.

https://doi.org/10.1017/jfm.2024.1200 Published online by Cambridge University Press

6.2.4. *Two-scale model with the small-scale spray model of synchronous droplets*

This case has been studied in § 4.3, where incompressible droplets oscillate synchronously for a given size. The dynamics has been derived respectively for each size of droplets using the weights and abscissas rather than the geometric quantities. Without losing the properties of the polydisperse case, we propose here to focus on the monodisperse case detailed in Appendix I. It allows a more compact equation of evolution for the small-scale interfacial area density $\Sigma = M^{\xi}_{1,0,0} + M^{\xi}_{1,2,0}$

$$\partial_t \Sigma + \boldsymbol{\nabla}\cdot(\Sigma \boldsymbol{u}) = \frac{16}{5}\frac{(\Delta\Sigma_\perp)(\Delta_t\Sigma_\perp)}{(n_1^d)^{1/3}(6\sqrt{\pi}\alpha_1^d)^{2/3}}. \tag{6.10}$$

Similarly to the previous cases, the incompressibility condition balances the isotropic terms to conserve α_1^d. Moreover, the right-hand side of (6.10) only accounts for the small-scale anisotropic motion such that

$$\left.\begin{aligned} \langle v_n \boldsymbol{n}\cdot\boldsymbol{\nabla}\boldsymbol{X}\rangle_E &= \alpha_1^d \boldsymbol{\nabla}\cdot\boldsymbol{u},\\ \langle \boldsymbol{\nabla}\cdot(v_n\boldsymbol{n})\delta_I\rangle_E &= -\Sigma\boldsymbol{\nabla}\cdot\boldsymbol{u},\\ \langle \boldsymbol{q}:\boldsymbol{\nabla}\boldsymbol{u}\rangle_E &= 0,\\ \langle \boldsymbol{q}:\boldsymbol{\nabla}(v_n\boldsymbol{n})\rangle_E &= -\frac{2}{(3\sqrt{4\pi})^{2/3}}\frac{(\Delta\Sigma_\perp)(\Delta_t\Sigma_\perp)}{(n_1^d)^{1/3}(\alpha_1^d)^{2/3}}. \end{aligned}\right\} \tag{6.11}$$

This last identification of closures concludes our approach where the dynamics is first assessed, and the geometry kinematics is obtained secondly. Our approach shows that for this last case, the dynamics cannot be simply expressed relying on the usual quantities α_1^d and Σ. The SAP modelling strategy allows the proper set of variables and conservation equations to be identified in the dynamical case, and a closed conservation equation to be obtained for the interface area density in particular, an important building block for further modelling such as evaporation or heat transfer.

7. Conclusion

In this work, we have proposed a novel framework to derive two-scale reduced-order models based on Hamilton's SAP as well as a set of geometric variables leading to the premises of a unified model for both disperse and separated phases two-phase flows, potentially including several dissipation phenomena. A hierarchy of small-scale models involving a variety of physical phenomena can be described within the framework.

The model is compatible in the two limits with classical models of the literature for disperse and separated two-phase flows and possesses essential properties for a proper mathematical framework, that is hyperbolicity and signed mathematical entropy evolution.

To deal with interface dynamics at small scale, we rely on GeoMOM: geometric variables are defined, which can be interpreted both as moments of a kinetic description at small scale, or as surface-averaged quantities, which are also defined in other regimes without any assumption on the geometry of the interface. This makes the link with the mixed zone and open new perspectives since we are able to tackle interface dynamics at small scale and reach a closed surface area density evolution equation for all the proposed small-scale models. It sheds some light on the fact that the natural variables to tackle the interface dynamics are not necessarily the interface area density and volume fractions but more intrinsic geometric quantities, the dynamics of which allow the interface area density evolution to be recovered.

Two issues have been left aside on purpose in the design of the paper for the sake of clarity of the exposition: (1) the existence of multiple velocities for the large-scale

https://doi.org/10.1017/jfm.2024.1200 Published online by Cambridge University Press

phases and for the disperse small scale as well as possible phase coupling through small-scale fluctuating velocities; and (2) the transfer of mass from large scale to small scale when capillarity is accounted for at all scales. The key issue is to include the related physics within the proposed framework. The first part is currently under investigation and relates to another version of the SAP with multiple velocities, while the second requires to include the capillarity at large scale and to interpret the transfer of scales as a local dissipative phenomenon; it is also the subject of a complementary piece of work (Loison *et al.* 2024). In the context of this latter contribution, special care must be given to the initialisation of the small-scale energy density to keep a global and consistent modelling of capillarity forces. Such effort is subject to ongoing investigations by the authors. Eventually, numerical methods also have to be designed in order to resolve properly the proposed models in the line of GeoMOM and preserve realisability. One last key issue is related to the treatment of small-scale agitation/turbulence of the large-scale phase, as mentioned in § 4, which would couple this velocity fluctuations to the droplet oscillations and provide sources terms in the kinetic equation. This is also the subject of our current investigation. This non-exhaustive list of extensions tends to assess the versatility of the proposed framework for the design of physically relevant and mathematically well-designed two-scale models for interfacial two-phase flows.

Acknowledgements. The discussions and insightful comments of R. Di Battista and F.-X. Demoulin are gratefully acknowledged.

Funding. This work has been funded by the French Department of Defence (Defence Innovation Agency) through the MMEED project. The PhD of A.L. is funded by a grant of the French Department of Higher Education and Research and the French Department of Defence (Defence Innovation Agency).

Declaration of interests. The authors report no conflict of interest.

Author ORCIDs.
Arthur Loison https://orcid.org/0009-0002-0001-996X;
Teddy Pichard https://orcid.org/0000-0002-9862-4019;
Samuel Kokh https://orcid.org/0000-0001-8685-4522;
Marc Massot https://orcid.org/0000-0001-8823-7667.

Appendix A. Condition of small-scale incompressibility in the disperse regime

We are interested in the compressibility caused by sound propagation at large scale. Consider then the two-scale mixture defined in § 2 with two large-scale liquid and gaseous phases and one small-scale liquid phase that share the same pressure P. Using $\kappa_T^k := \rho_k^{-1}(\partial\rho_k/\partial P)_T$ to denote the isothermal compressibility, we measure the mixture compressibility using the mass conservation of each phase with

$$\boldsymbol{\nabla}\cdot\boldsymbol{u} = \sum_{k=1,2,1^d} \alpha_k \boldsymbol{\nabla}\cdot\boldsymbol{u} = -\sum_{k=1,2,1^d} \alpha_k \frac{D_t\rho_k}{\rho_k} = -\sum_{k=1,2,1^d} \alpha_k \kappa_T^k D_t P. \tag{A1}$$

The liquid phase is much less compressible than the gaseous phases $\kappa_T^1, \kappa_T^{1,d} \ll \kappa_T^2$. Moreover, the small-scale liquid phase only occupies a small amount of the mixture volume $\alpha_1^d \ll \alpha_1, \alpha_2$. Then, the contributions to the overall compressibility of the mixture are ranked like

$$|\alpha_2\kappa_T^2 D_t P| \gg |\alpha_1\kappa_T^1 D_t P| \gg |\alpha_1^d\kappa_T^{1,d} D_t P|. \tag{A2}$$

The small-scale liquid phase can then be assumed incompressible in comparison to both large-scale phases.

https://doi.org/10.1017/jfm.2024.1200 Published online by Cambridge University Press

Appendix B. Stationary action principle

B.1. *Derivation of the conservative dynamics*

Consider the Lagrangian defined in (2.13),

$$\mathcal{L} = \mathcal{L}_1(\alpha_1, m_1, \boldsymbol{u}) + \mathcal{L}_2(\alpha_2, m_2, \boldsymbol{u}) + \mathcal{L}_1^d(m_1^d, \rho_1^d, \zeta, \boldsymbol{u}). \tag{B1}$$

The dependency on $\rho_1^d = m_1^d/\alpha_1^d$ was added to take advantage of the constraint $D_t\rho_1^d = 0$ in the derivation with Hamilton's SAP. Then, the dependencies of the small-scale Lagrangian are $\mathcal{L}_1^d = \frac{1}{2}m_1^d\boldsymbol{u}^2 - m_1^d e_1(\rho_1^d) - m_1^d\zeta$.

Hamilton's SAP provides the momentum equation by minimising the Lagrangian's action, i.e. the integral of the Lagrangian over a space domain $\Omega_{\boldsymbol{x}}$ and a time interval $[0, T]$. This minimisation takes place under the mass conservation (2.7) and incompressibility constraints (2.10). We minimise the action of the whole mixture defined by

$$\mathcal{A} = \int_{\Omega} \mathcal{L}\,\mathrm{d}\boldsymbol{x}\,\mathrm{d}t, \tag{B2}$$

where $\boldsymbol{x}$ is the position in Eulerian coordinates and $\Omega := \Omega_{\boldsymbol{x}} \times [0, T]$ is the Eulerian space–time domain. This minimisation is performed over a family of trajectories defined by Lagrangian mappings $\boldsymbol{\phi}^\lambda(\boldsymbol{X}, t, \lambda)$ parametrised by λ which lies in the vicinity of 0 and $\boldsymbol{X} = \boldsymbol{\phi}^{-1}(\boldsymbol{x}, t)$ the Lagrangian coordinates. We similarly introduce families of Eulerian fields $\alpha_1^\lambda(\boldsymbol{x}, t, \lambda)$, $b_c^\lambda(\boldsymbol{x}, t, \lambda)$, $b_a^\lambda(\boldsymbol{x}, t, \lambda)$ for the volume fraction, the conserved variables and the advected ones. We assume that these families of Lagrangian mappings and Eulerian fields satisfy the following conditions.

(i) The mapping and Eulerian fields of the solution is included in the families for $\lambda = 0$, i.e. for all $(\boldsymbol{x}, t) \in \Omega$,

$$\alpha_1^\lambda(\boldsymbol{x}, t, \lambda = 0) = \alpha_1(\boldsymbol{x}, t), \quad b_c^\lambda(\boldsymbol{x}, t, \lambda = 0) = b_c(\boldsymbol{x}, t), \quad b_a^\lambda(\boldsymbol{x}, t, \lambda = 0) = b_a(\boldsymbol{x}, t). \tag{B3a–c}$$

(ii) All the mappings and Eulerian fields preserve the constraints, i.e. for all $(\boldsymbol{x}, t) \in \Omega$,

$$\partial_t b_c^\lambda + \boldsymbol{\nabla}\cdot(b_c^\lambda\boldsymbol{u}) = 0, \quad \partial_t b_a^\lambda + \boldsymbol{u}\cdot\boldsymbol{\nabla} b_a^\lambda = 0. \tag{B4a,b}$$

(iii) All the mappings and Eulerian fields preserve the values at boundaries of the space–time domain, i.e. for all $(\boldsymbol{x}, t) \in \partial\Omega$,

$$\alpha_1^\lambda(\boldsymbol{x}, t, \lambda) = \alpha_1(\boldsymbol{x}, t), \quad b_c^\lambda(\boldsymbol{x}, t, \lambda) = b_c(\boldsymbol{x}, t), \quad b_a^\lambda(\boldsymbol{x}, t, \lambda) = b_a(\boldsymbol{x}, t). \tag{B5a–c}$$

We define the following variations,

$$\boldsymbol{\eta}(\boldsymbol{x}, t) := (\partial_\lambda\boldsymbol{\phi}^\lambda)_{X,t}(\boldsymbol{\phi}^{-1}(\boldsymbol{x}, t), t, \lambda = 0), \quad \delta b_e(\boldsymbol{x}, t) := (\partial_\lambda b_e^\lambda)_{\boldsymbol{x},t}(\boldsymbol{x}, t, \lambda = 0), \tag{B6a,b}$$

where $\boldsymbol{\eta}$ is an infinitesimal Eulerian displacement and δb_e the variation on any Eulerian field b_e. With this variational operator, Hamilton's SAP can be simply written as

$$\delta\mathcal{A} = 0. \tag{B7}$$

Following Truskinovsky (1991), Gavrilyuk *et al.* (1998), Gouin & Gavrilyuk (1999), Gavrilyuk & Saurel (2002), Drui *et al.* (2019), Gouin (2020) and Cordesse *et al.* (2020*a*), the variations of b_c, b_a and $\boldsymbol{u}$ are related to $\boldsymbol{\eta}$ through relations

$$\delta b_c = -\boldsymbol{\nabla}\cdot(b_c\boldsymbol{\eta}), \quad \delta b_a = -(\boldsymbol{\eta}\cdot\boldsymbol{\nabla})b_a, \quad \delta\boldsymbol{u} = D_t\boldsymbol{\eta} - (\boldsymbol{\eta}\cdot\boldsymbol{\nabla})\boldsymbol{u}. \tag{B8a–c}$$

For the Lagrangian under consideration, we have $b_c \in \{m_1, m_2, m_1^d, \alpha_1^d\}$ and advected quantities $b_a \in \{\rho_1^d\}$. The variation of α_2 is linked to both $\boldsymbol{\eta}$ and $\delta\alpha_1$ through the

https://doi.org/10.1017/jfm.2024.1200 Published online by Cambridge University Press

volume occupation relation $\alpha_2 = 1 - \alpha_1 - \alpha_1^d$. With the summation on repeated indexes, we define the divergence of $\boldsymbol{A}$ by $\nabla \cdot \boldsymbol{A} = (\partial_{x_j} A_{ij})$ and the gradient of a vector $\nabla \boldsymbol{b} = (\partial_{x_i} b_j)$. We decompose the action variation in Eulerian coordinates with respect to each dependency

$$\delta\mathcal{A}_{\alpha_1} = \int_\Omega \partial_{\alpha_1}\mathcal{L}_1 \delta\alpha_1, \tag{B9}$$

$$\delta\mathcal{A}_{\alpha_2} = \int_\Omega \partial_{\alpha_2}\mathcal{L}_2 \delta\alpha_2 = -\int_\Omega \alpha_1^d \nabla(\partial_{\alpha_2}\mathcal{L}_2)\cdot\boldsymbol{\eta} - \int_\Omega \partial_{\alpha_2}\mathcal{L}_2\delta\alpha_1, \tag{B10}$$

$$\delta\mathcal{A}_{m_k} = \int_\Omega \partial_{m_k}\mathcal{L}_k \delta m_k = \int_\Omega m_k \nabla(\partial_{m_k}\mathcal{L}_k)\cdot\boldsymbol{\eta}, \tag{B11}$$

$$\delta\mathcal{A}_{\rho_1^d} = \int_\Omega -\partial_{\rho_1^d}\mathcal{L}_1^d \nabla\rho_1^d \cdot \boldsymbol{\eta}, \tag{B12}$$

$$\delta\mathcal{A}_{\zeta} = \int_\Omega -\partial_{\zeta}\mathcal{L}_1^d \nabla\zeta \cdot \boldsymbol{\eta}, \tag{B13}$$

$$\delta\mathcal{A}_{\boldsymbol{u}} = \int_\Omega -(\partial_t \boldsymbol{K} + \nabla\cdot(\boldsymbol{K}\otimes\boldsymbol{u}) + \boldsymbol{K}\cdot\nabla\boldsymbol{u})\cdot\boldsymbol{\eta}, \tag{B14}$$

where $\delta\alpha_1^d$ follows (B8), $\delta\alpha_2 = -\delta\alpha_1 - \delta\alpha_1^d$ and $\boldsymbol{K} = \partial_{\boldsymbol{u}}\mathcal{L}$. Remark that we denoted here the matrix–vector product of a matrix $\boldsymbol{A}$ with a vector $\boldsymbol{b}$ by $\boldsymbol{b}\cdot\boldsymbol{A} = (A_{ij}b_j)$. Denoting $\mathcal{L}_k^* = m_k(\partial_{m_k}\mathcal{L}_k) - \mathcal{L}_k$ and $\mathcal{L}^* = \sum_k \mathcal{L}_k^*$, then $\delta\mathcal{A}$ can be expressed as a combination of variations $\boldsymbol{\eta}$ and $\delta\alpha_1$,

$$\begin{aligned}
\delta\mathcal{A} = &-\int_\Omega (\partial_t\boldsymbol{K} + \nabla\cdot(\boldsymbol{K}\otimes\boldsymbol{u}) + \boldsymbol{K}\cdot\nabla\boldsymbol{u} + \alpha_1^d\nabla(\partial_{\alpha_2}\mathcal{L}_2) + \partial_{\rho_1^d}\mathcal{L}_1^d\nabla\rho_1^d + \partial_\zeta\mathcal{L}_1^d\nabla\zeta \\
&- m_1\nabla(\partial_{m_1}\mathcal{L}_1) - m_2\nabla(\partial_{m_2}\mathcal{L}_2) - m_1^d\nabla(\partial_{m_1^d}\mathcal{L}_1^d))\cdot\boldsymbol{\eta} \\
&+ \int_\Omega (\partial_{\alpha_1}\mathcal{L}_1 - \partial_{\alpha_2}\mathcal{L}_2)\delta\alpha_1, \\
= &-\int_\Omega (\partial_t\boldsymbol{K} + \nabla\cdot(\boldsymbol{K}\otimes\boldsymbol{u}) - \nabla(\mathcal{L}^* - \alpha_1^d\partial_{\alpha_2}\mathcal{L}_2) - (\partial_{\alpha_1}\mathcal{L}_1 - \partial_{\alpha_2}\mathcal{L}_2)\nabla\alpha_1)\cdot\boldsymbol{\eta} \\
&+ \int_\Omega (\partial_{\alpha_1}\mathcal{L}_1 - \partial_{\alpha_2}\mathcal{L}_2)\delta\alpha_1,
\end{aligned} \tag{B15}$$

with $\boldsymbol{K} = \partial_{\boldsymbol{u}}\mathcal{L}$ and $\mathcal{L}_k^* = m_k(\partial_{m_k}\mathcal{L}_k) - \mathcal{L}_k$. The fundamental theorem of variations applied to (B15) gives

$$\delta\mathcal{A} = 0 \Rightarrow \begin{cases} \partial_t\boldsymbol{K} + \nabla\cdot(\boldsymbol{K}\otimes\boldsymbol{u}) - \nabla(\mathcal{L}^* - \alpha_1^d\partial_{\alpha_2}\mathcal{L}_2) = 0, \\ \partial_{\alpha_1}\mathcal{L}_1 - \partial_{\alpha_2}\mathcal{L}_2 = 0. \end{cases} \tag{B16}$$

Developing the expression of the derivatives yields (2.14).

https://doi.org/10.1017/jfm.2024.1200 Published online by Cambridge University Press

B.2. *Additional conservation equation*

Starting from (2.14), we now look for an additional conservation equation on $\mathcal{H} = \boldsymbol{K} \cdot \boldsymbol{u} - \mathcal{L}$. We take the scalar product of the momentum equation with $\boldsymbol{u}$ to get

$$\begin{aligned} 0 &= \partial_t(\boldsymbol{K}\cdot\boldsymbol{u}) - \boldsymbol{K}\partial_t\boldsymbol{u} + \boldsymbol{\nabla}\cdot((\boldsymbol{K}\cdot\boldsymbol{u})\boldsymbol{u}) - \boldsymbol{K}(\boldsymbol{u}\cdot\boldsymbol{\nabla})\boldsymbol{u} - \boldsymbol{\nabla}\cdot(p\boldsymbol{u}) - p\boldsymbol{\nabla}\cdot\boldsymbol{u} \\ &= \partial_t\mathcal{H} + \boldsymbol{\nabla}\cdot((\mathcal{H}+p)\boldsymbol{u}) + \partial_t\mathcal{L} - \boldsymbol{K}D_t\boldsymbol{u} + \boldsymbol{\nabla}\cdot(\mathcal{L}\boldsymbol{u}) - p\boldsymbol{\nabla}\cdot\boldsymbol{u} \\ &= \partial_t\mathcal{H} + \boldsymbol{\nabla}\cdot((\mathcal{H}+p)\boldsymbol{u}) + D_t\mathcal{L} - \boldsymbol{K}D_t\boldsymbol{u} + (\mathcal{L}-p)\boldsymbol{\nabla}\cdot\boldsymbol{u}. \end{aligned} \tag{B17}$$

We develop the material time derivative and isolate the mass and incompressibility constraints such that (B17) becomes

$$\begin{aligned} 0 &= \partial_t\mathcal{H} + \boldsymbol{\nabla}\cdot((\mathcal{H} - (\mathcal{L}^* - \alpha_1^d\partial_{\alpha_2}\mathcal{L}_2))\boldsymbol{u}) + (\mathcal{L}-p)\boldsymbol{\nabla}\cdot\boldsymbol{u} \\ &\quad + \partial_{\alpha_1}\mathcal{L}_1 D_t\alpha_1 + \partial_{\alpha_2}\mathcal{L}_2 D_t\alpha_2 + \partial_{\rho_1^d}\mathcal{L}_1^d D_t\rho_1^d + \partial_\zeta\mathcal{L}_1^d D_t\zeta \\ &\quad + \partial_{m_1}\mathcal{L}_1 D_t m_1 + \partial_{m_2}\mathcal{L}_2 D_t m_2 + \partial_{m_1^d}\mathcal{L}_1^d D_t m_1^d \\ &= \partial_t\mathcal{H} + \boldsymbol{\nabla}\cdot((\mathcal{H}+p)\boldsymbol{u}) + (\mathcal{L} - m_1\partial_{m_1}\mathcal{L}_1 - m_2\partial_{m_2}\mathcal{L}_2 - m_1^d\partial_{m_1^d}\mathcal{L}_1^d - p)\boldsymbol{\nabla}\cdot\boldsymbol{u} \\ &\quad + \partial_{\alpha_1}\mathcal{L}_1 D_t\alpha_1 + \partial_{\alpha_2}\mathcal{L}_2 D_t\alpha_2 + \partial_{\rho_1^d}\mathcal{L}_1^d D_t\rho_1^d + \partial_\zeta\mathcal{L}_1^d D_t\zeta \\ &\quad + \partial_{m_1}\mathcal{L}_1(\partial_t m_1 + \boldsymbol{\nabla}\cdot(m_1\boldsymbol{u})) + \partial_{m_2}\mathcal{L}_2(\partial_t m_2 + \boldsymbol{\nabla}\cdot(m_2\boldsymbol{u})) \\ &\quad + \partial_{m_1^d}\mathcal{L}_1^d(\partial_t m_1^d + \boldsymbol{\nabla}\cdot(m_1^d\boldsymbol{u})). \end{aligned} \tag{B18}$$

The four last terms nullify thanks to the constraints while we develop $D_t\alpha_2$ using the volume occupation constraint $\alpha_1 + \alpha_2 + \alpha_1^d = 1$ and the conservation of α_1^d. It yields

$$\begin{aligned} 0 &= \partial_t\mathcal{H} + \boldsymbol{\nabla}\cdot((\mathcal{H}+p)\boldsymbol{u}) - (p+\mathcal{L}^*)\boldsymbol{\nabla}\cdot\boldsymbol{u} + (\partial_{\alpha_1}\mathcal{L}_1 - \partial_{\alpha_2}\mathcal{L}_2)D_t\alpha_1 - \partial_{\alpha_2}\mathcal{L}_2 D_t\alpha_1^d \\ &= \partial_t\mathcal{H} + \boldsymbol{\nabla}\cdot((\mathcal{H}+p)\boldsymbol{u}) - (p + \mathcal{L}^* - \alpha_1^d\partial_{\alpha_2}\mathcal{L}_2)\boldsymbol{\nabla}\cdot\boldsymbol{u} + (\partial_{\alpha_1}\mathcal{L}_1 - \partial_{\alpha_2}\mathcal{L}_2)D_t\alpha_1. \end{aligned} \tag{B19}$$

Finally, the pressure equilibrium given by the second equation of (B16) gives

$$\mathcal{L}^* + \alpha_1^d\partial_{\alpha_2}\mathcal{L}_2 = -p, \tag{B20}$$

and we obtain the desired conservation equation on $\mathcal{H}$.

Appendix C. Dimensionless analysis of the dissipative two-scale model

We consider here the two-scale model with dissipative pressure relaxation (2.22) together with the Stokes viscosity term (2.23). We introduce the following dimensionless variables

$$\left.\begin{aligned} \boldsymbol{\nabla}^* = L_{ref}\boldsymbol{\nabla}, \quad \boldsymbol{u}^* = \frac{\boldsymbol{u}}{u_{ref}}, \quad t^* = t\frac{u_{ref}}{L_{ref}}, \quad \rho^* = \frac{\rho}{\rho_{ref}}, \\ p^* = \frac{p}{\rho_{ref}(c_F^d)^2} \quad \text{for } p = \bar{p}, p_1, p_2. \end{aligned}\right\} \tag{C1}$$

https://doi.org/10.1017/jfm.2024.1200 Published online by Cambridge University Press

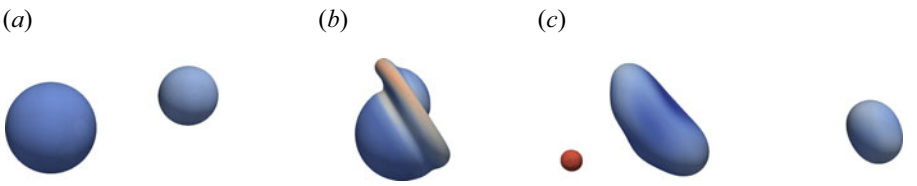


Figure 2. Local mean curvature for the collision of two droplets that scales between $H_{min} = 6.3 \times 10^2$ m^{-1} (blue) and $H_{max} = 2.4 \times 10^4$ m^{-1} (red): (*a*) before the collision, (*b*) beginning of the collision and (*c*) after the collision.

Then, it yields the following dimensionless set of equations

$$\left.\begin{aligned}
&\partial_{t^*} m_k + \boldsymbol{\nabla}^* \cdot (m_k \boldsymbol{u}^*) = 0 \quad \text{for } k = 1, 2, 1^d, \\
&\partial_{t^*} \alpha_1^d + \boldsymbol{\nabla}^* \cdot (\alpha_1^d \boldsymbol{u}^*) = 0, \\
&\partial_{t^*} (\rho^* \boldsymbol{u}^*) + \boldsymbol{\nabla}^* \cdot (\rho^* \boldsymbol{u}^* \otimes \boldsymbol{u}^*) \\
&\quad = -\frac{1}{Ma^2} \boldsymbol{\nabla}^* \bar{p}^* + \frac{1}{Re_\mu} \boldsymbol{\nabla}^* \cdot ((\boldsymbol{\nabla}^* \boldsymbol{u}^* + (\boldsymbol{\nabla}^* \boldsymbol{u}^*)^T)) + \frac{1}{Re_\lambda} \boldsymbol{\nabla}^* \cdot ((\boldsymbol{\nabla}^* \cdot \boldsymbol{u}^*) \boldsymbol{I}), \\
&D_{t^*} \bar{\alpha}_1 = Ma^2 Re_\epsilon (p_1^* - p_2^*),
\end{aligned}\right\} \tag{C2}$$

with the Mach number $Ma = u_{ref}/c_F^d$ and the Reynolds number $Re_X = \rho_{ref} L_{ref} u_{ref}/X$ for a given dynamic viscosity X. In the context of two-phase flow atomisation, one can typically encounter regimes with high velocities $Ma \approx 1$ and high Reynolds numbers $Re_\mu, Re_\lambda, Re_\epsilon \ll 1$. Large-scale capillarity is here not modelled but corresponds also to high Weber number. Such context is here retained in the remainder of the paper as it also lightens the calculations.

Appendix D. Large-scale and small-scale geometry description using GeoMOM geometric quantities

We propose here to illustrate why the choice of small-scale variables, which are at the same time moments of a kinetic modelling level as well as surface-averaged geometric quantities is fundamentally convenient for two-scale modelling. As their definitions are based on the surface-average operator in § 3, they can be computed for any flow topology beyond any assumption on the geometry and dynamics of the interface.

We illustrate this point by comparing the evaluation of such quantities in a single realisation of the collision of two droplets at small scale.

The simulation has been performed with the ARCHER code (Ménard, Tanguy & Berlemont 2007) (see details in Essadki *et al.* 2019) with $256 \times 256 \times 512$ cells in a volume V_{tot} of 1 mm $\times$ 1mm $\times$ 2 mm and the geometric post-treatment of the obtained level set is done with the open-source library Mercur(v)e, which relies on a triangulation of the interface as well as geometric properties preserving the topological invariants (Cordesse *et al.* 2020*a*). Before the collision, the two droplets are spherical with diameters of 400 and 260 µm (see figure 2*a*). After the collision, there are three deformed inclusions with different sizes (see figure 2*c*).

We usually consider a kinetic description at mesoscopic level based on a statistical ensemble average of several realisations, but for the purpose of the present illustration we stick to a single realisation, since the kinetic description (3.2) is also valid in this case of measure-valued number distribution functions. At the kinetic level of description, we

https://doi.org/10.1017/jfm.2024.1200 Published online by Cambridge University Press

	α_1^d	Σ	$\Sigma\langle H\rangle$	$\Sigma\langle G\rangle$
Before collision	2.14×10^{-2}	3.57×10^{2} m^{-1}	2.1×10^{6} m^{-2}	1.3×10^{10} m^{-3}
After collision	2.14×10^{-2}	3.91×10^{2} m^{-1}	2.5×10^{6} m^{-2}	1.9×10^{10} m^{-3}

(*a*) Geometric quantities before and after the collision.

	$n_1 \times V_{tot}$	$(S_0)_1$	$n_2 \times V_{tot}$	$(S_0)_2$
Before collision	1	2.12×10^{-7} m^2	1	5.03×10^{-7} m^2
After collision	0.76	1.38×10^{-8} m^2	2.24	3.4×10^{-7} m^2

(*b*) Weights (nb. of droplets) in the domain of volume V_{tot}, and abscissas before and after the collision.

Table 1. Values of each geometric variable before and after collision, from the analytical initial configuration and the geometric post-treatment, respectively, along with the corresponding weights and abscissas of (D1).

reconstruct the distribution using the two-point quadrature

$$n_{S_0}(\hat{S}_0) = n_1\delta(\hat{S}_0 - (S_0)_1) + n_2\delta(\hat{S}_0 - (S_0)_2). \tag{D1}$$

We could also have used another reconstruction techniques such as the entropy maximisation technique (Mead & Papanicolaou 1984; Levermore 1996; Essadki *et al.* 2018), which maximises the concave functional $n \mapsto -n\log n$, while constraining the values of some selected moments. Such techniques are better suited for statistical descriptions corresponding to many realisations/inclusions or when a smooth NDF is required, such as when evaporation is taking place. We gather in table 1(*a*,*b*) the values of each geometric variable before and after collision, from the analytical initial configuration and the geometric post-treatment, respectively, along with the corresponding weights and abscissas of (D1). Let us study the reconstruction of the NDF is well-predicted through the chosen moments, showing how to interpret the chosen geometric variables. Before the collision, (D1) has the exact number of parameters to represent well the two droplets. After the collision, droplets' sizes are sensitively changed with a droplet much smaller than the other two. With Mercur(v)e, the geometric invariant associated surface-averaged Gauss curvature is well-preserved and recovers well the total number of droplets. However, (D1) has not enough parameters to detect three different sizes, even less the deformations. However, deformations could be better modelled if we switched to the eight-moment model. Nevertheless, even if it is a reduced-order model, the retained key information about the geometry at small scale allow us to always have a representation, through quadrature, of a small-scale interface.

Let us conclude this illustration by underlining that the above results correspond to a treatment of the interface geometry as small scale. We could also have taken the point of view of the large scale, where all the geometry is not obtained through a geometric post-treatment, but can be locally estimated relying on $\bar{\alpha}_1$ only. For instance, the interface area density and the mean curvature can be estimated using $\|\nabla\bar{\alpha}_1\|$ and $\nabla\cdot(\nabla\bar{\alpha}_1/\|\nabla\bar{\alpha}_1\|)$ (Goldman 2005), as long as the characteristic lengths stay at large-scale, that is above a given threshold.

https://doi.org/10.1017/jfm.2024.1200 Published online by Cambridge University Press

Appendix E. Derivation of the model for the polydisperse spray of incompressible droplets

We consider here the two-scale model with capillarity at the small scale modelled by a polydisperse spray of spherical and incompressible droplets. The Lagrangian of the mixture is given by (2.13) with the modified small-scale Lagrangian given by (3.13) and reads

$$\mathcal{L} = \mathcal{L}_1(\alpha_1, m_1, \boldsymbol{u}) + \mathcal{L}_2(\alpha_2, m_2, \boldsymbol{u}) + \mathcal{L}_1^d(m_1^d, \rho_1^d, z, \boldsymbol{u}), \tag{E1}$$

where $z = \Sigma/m_1^d$ has a similar role to the variable defined in Appendix A as $D_t z = 0$. Moreover, ρ_1^d is constrained by $D_t \rho_1^d = 0$ and α_1^d is conserved such that the action, as defined in Appendix B, is decomposed according to each dependency,

$$\delta\mathcal{A}_{\alpha_1} = \int_\Omega \partial_{\alpha_1}\mathcal{L}_1 \delta\alpha_1, \tag{E2}$$

$$\delta\mathcal{A}_{\alpha_2} = \int_\Omega \partial_{\alpha_2}\mathcal{L}_2 \delta\alpha_2 = -\int_\Omega \alpha_1^d \boldsymbol{\nabla}(\partial_{\alpha_2}\mathcal{L}_2)\cdot\boldsymbol{\eta} - \int_\Omega \partial_{\alpha_2}\mathcal{L}_2\delta\alpha_1, \tag{E3}$$

$$\delta\mathcal{A}_{m_k} = \int_\Omega \partial_{m_k}\mathcal{L}_k \delta m_k = \int_\Omega m_k \boldsymbol{\nabla}(\partial_{m_k}\mathcal{L}_k)\cdot\boldsymbol{\eta}, \tag{E4}$$

$$\delta\mathcal{A}_{\rho_1^d} = \int_\Omega -\partial_{\rho_1^d}\mathcal{L}_1^d \boldsymbol{\nabla}\rho_1^d \cdot \boldsymbol{\eta}, \tag{E5}$$

$$\delta\mathcal{A}_z = \int_\Omega -\partial_z \mathcal{L}_1^d \boldsymbol{\nabla} z \cdot \boldsymbol{\eta}, \tag{E6}$$

$$\delta\mathcal{A}_{\boldsymbol{u}} = \int_\Omega -(\partial_t \boldsymbol{K} + \boldsymbol{\nabla}\cdot(\boldsymbol{K}\otimes\boldsymbol{u}) + \boldsymbol{K}\cdot\boldsymbol{\nabla}\boldsymbol{u})\cdot\boldsymbol{\eta}. \tag{E7}$$

The variation of the total action can then be written as

$$\begin{aligned}
\delta\mathcal{A} = &-\int_\Omega (\partial_t \boldsymbol{K} + \boldsymbol{\nabla}\cdot(\boldsymbol{K}\otimes\boldsymbol{u}) + \boldsymbol{K}\cdot\boldsymbol{\nabla}\boldsymbol{u} + \alpha_1^d\boldsymbol{\nabla}(\partial_{\alpha_2}\mathcal{L}_2) + \partial_z\mathcal{L}_1^d\boldsymbol{\nabla} z \\
&- m_1\boldsymbol{\nabla}(\partial_{m_1}\mathcal{L}_1) - m_2\boldsymbol{\nabla}(\partial_{m_2}\mathcal{L}_2) - m_1^d\boldsymbol{\nabla}(\partial_{m_1^d}\mathcal{L}_1^d))\cdot\boldsymbol{\eta} \\
&+ \int_\Omega (\partial_{\alpha_1}\mathcal{L}_1 - \partial_{\alpha_2}\mathcal{L}_2)\delta\alpha_1, \\
= &-\int_\Omega (\partial_t \boldsymbol{K} + \boldsymbol{\nabla}\cdot(\boldsymbol{K}\otimes\boldsymbol{u}) - \boldsymbol{\nabla}(\mathcal{L}^* - \alpha_1^d\partial_{\alpha_2}\mathcal{L}_2) - (\partial_{\alpha_1}\mathcal{L}_1 - \partial_{\alpha_2}\mathcal{L}_2)\boldsymbol{\nabla}\alpha_1)\cdot\boldsymbol{\eta} \\
&+ \int_\Omega (\partial_{\alpha_1}\mathcal{L}_1 - \partial_{\alpha_2}\mathcal{L}_2)\delta\alpha_1.
\end{aligned} \tag{E8}$$

Nullifying the variations gives the following system

$$\left.\begin{aligned} \partial_t \boldsymbol{K} + \boldsymbol{\nabla}\cdot(\boldsymbol{K}\otimes\boldsymbol{u}) - \boldsymbol{\nabla}(\mathcal{L}^* - \alpha_1^d\partial_{\alpha_2}\mathcal{L}_2) = 0, \\ \partial_{\alpha_1}\mathcal{L}_1 - \partial_{\alpha_2}\mathcal{L}_2 = 0. \end{aligned}\right\} \tag{E9}$$

We replace then the derivatives of the Lagrangian by their expressions

$$\partial_{\boldsymbol{u}}\mathcal{L} = \boldsymbol{K} = \rho\boldsymbol{u}, \quad \mathcal{L}^* = -\alpha_1 p_1 - \alpha_2 p_2, \quad \partial_{\alpha_2}\mathcal{L}_2 = p_2, \quad \partial_{\alpha_1}\mathcal{L}_1 = p_1. \tag{E10a–d}$$

https://doi.org/10.1017/jfm.2024.1200 Published online by Cambridge University Press

Then, (E9) becomes

$$\left.\begin{array}{c}\partial_t(\rho \boldsymbol{u}) + \boldsymbol{\nabla} \cdot (\rho \boldsymbol{u} \otimes \boldsymbol{u} + p\boldsymbol{I}) = 0, \\ p := p_1 = p_2.\end{array}\right\} \tag{E11}$$

Appendix F. Results of differential geometry

We recall here some elements to derive the evolution in time of the geometry for closed inclusions using the tools of differential geometry. The reader is referred to Kreyszig (1991) for a general introduction to differential geometry and to Capovilla, Guven & Santiago (2003) and Deserno (2015) for a briefer introduction and the derivation of the formulae presented hereafter.

F.1. *First- and second-order variations of a closed inclusion*

Let us consider the deformation of a closed inclusion defined by its position vector mapped by $\mathcal{U}$

$$\boldsymbol{r}(u, v) = \boldsymbol{r}_0(u, v) + \delta \boldsymbol{r}(u, v), \quad (u, v) \in \mathcal{U}, \tag{F1}$$

where $\boldsymbol{r}_0$ is the position before the deformation and $\delta \boldsymbol{r}$ the deformation vector that we assume to be small. From now on, we drop the dependencies on (u, v) to lighten the formulae. For convex and closed inclusions, we write the deformation in the direction of the non-deformed surface normal,

$$\boldsymbol{r} = \boldsymbol{r}_0 + \psi \boldsymbol{n}, \tag{F2}$$

where $\boldsymbol{n} := (\boldsymbol{e}_\theta \times \boldsymbol{e}_\phi)/\|\boldsymbol{e}_\theta \times \boldsymbol{e}_\phi\|$ is the local normal and $\boldsymbol{e}_a := \partial_a \boldsymbol{r}$ the tangential vectors and ψ the local amplitude of the deformation. Then, we are interested in the first-order and second-order variations of particular geometric quantities of the whole inclusion. With the surface-weighted average operator $\widetilde{(\cdot)}$ defined in (3.3) for one inclusion, we focus on the volume V, the surface area S and the surface-weighted mean curvature $S\tilde{H}$. There is no variation associated with the surface-weighted Gauss curvature $S\tilde{G}$ as a result of the Gauss–Bonnet theorem (Kreyszig 1991). The variations of these quantities up to second order in ψ are found in Capovilla *et al.* (2003) and written with the Einstein summation rule for implicit indexes $a, b \in \{u, v\}$,

$$\left.\begin{array}{c}\delta V = \displaystyle\int_{\mathcal{U}} (\psi + H_0\psi^2)A_0 + o(\psi^2), \\ \delta S = \displaystyle\int_{\mathcal{U}} \left(2H_0\psi + G_0\psi^2 - \frac{1}{2}\psi\Delta\psi\right)A_0 + o(\psi^2), \\ \delta(S\tilde{H}) = \displaystyle\int_{\mathcal{U}} \left(G_0\psi + \frac{1}{2}\psi[(\boldsymbol{K}^{ab} - 2H_0\boldsymbol{g}^{ab}) : (\boldsymbol{\nabla}_a \otimes \boldsymbol{\nabla}_b)\psi - \boldsymbol{G} : \boldsymbol{K}^{ab}\psi]\right)A_0 + o(\psi^2),\end{array}\right\} \tag{F3}$$

where H_0 and G_0 are the non-deformed mean and Gauss curvature, Δ is the surface Laplacian, $\boldsymbol{K}^{ab}$ the extrinsic curvature tensor, $\boldsymbol{g}^{ab}$ the inverse of the metric tensor, $\boldsymbol{\nabla}_a$ is the vector of covariant derivative with respect to a and $\boldsymbol{G}$ the Einstein tensor.

https://doi.org/10.1017/jfm.2024.1200 Published online by Cambridge University Press

F.2. *Incompressible oscillation of the sphere*

In § 4, we are specifically interested in a sphere deformed by the axisymmetric second spherical harmonic. We choose the spherical coordinates $(u, v) = (\theta, \phi)$ on $\mathcal{U} = (0, \pi) \times (0, 2\pi)$, and we denote $\boldsymbol{e}_r = (\sin\theta\cos\phi, \sin\theta\sin\phi, \cos\theta)$ such that

$$\boldsymbol{r}_0 = R_0\boldsymbol{e}_r, \quad \psi(\theta, \phi) = x_0 Y_0 + x_2 Y_2(\theta), \tag{F4a,b}$$

where R_0 is the constant radius of the non-deformed sphere, Y_0 is the zeroth spherical harmonic that corresponds to the isotropic perturbation that ensures incompressibility and Y_2 is the second spherical harmonic associated with the oscillatory motion. Then, we evaluate the geometric quantities in (F3),

$$\left.\begin{array}{rrrrr} \boldsymbol{n} = \boldsymbol{e}_r, & H_0 = R_0^{-1}, & G_0 = R_0^{-2}, & A_0 = R_0^2 A_{\mathbb{S}^2}, & \\ \boldsymbol{K}^{ab} = R_0^{-1}\boldsymbol{g}^{ab}, & \boldsymbol{g}^{ab} : \nabla_a \otimes \nabla_b = \Delta, & \Delta = R_0^{-2}\Delta_{\mathbb{S}^2}, & \boldsymbol{G} = \boldsymbol{0}, & \end{array}\right\} \tag{F5}$$

where $\Delta_{\mathbb{S}^2}$ and $A_{\mathbb{S}^2}$ are the surface Laplacian and the surface element on the unit sphere $\mathbb{S}^2$. Furthermore, the orthonormal spherical harmonics Y_0 and Y_2 are eigenfunctions of the spherical Laplacian $\Delta_{\mathbb{S}^2}$ such that

$$\Delta_{\mathbb{S}^2} Y_k = -k(k+1)Y_k, \quad \int_{\mathcal{U}} Y_k Y_{k'} A_{\mathbb{S}^2} = \delta_{k,k'}. \tag{F6a,b}$$

Evaluating the variations of V, S and $S\tilde{H}$ up to second order in x_0 and x_2 yields

$$\left.\begin{aligned} \delta V &= R_0^2 x_0 + R_0 x_0^2 + R_0 x_2^2 + o(x_0^2 + x_2^2), \\ \delta S &= 2R_0 x_0 + x_0^2 + 4x_2^2 + o(x_0^2 + x_2^2), \\ \delta(S\tilde{H}) &= x_0 + 3R_0^{-1}x_2^2 + o(x_0^2 + x_2^2). \end{aligned}\right\} \tag{F7}$$

As we consider incompressible oscillations $\delta V = 0$, this links the dynamics of x_0 to that of x_2

$$\delta V = 0 \;\Rightarrow\; x_0 = -R_0^{-1}x_2^2 + o(x_2^2). \tag{F8}$$

The variations of the geometric quantities then simplify to

$$\delta V = 0, \quad \delta S = 2x_2^2 + o(x_2^2), \quad \delta(S\tilde{H}) = 2R_0^{-1}x_2^2 + o(x_2^2). \tag{F9a–c}$$

We then obtain (4.6) by introducing $S_0 = 4\pi R_0^2$ and $\chi = x_2(2/S_0)^{1/2}$.

F.3. *Variations of the oriented geometric quantities*

In § 4.3, new geometric quantities $S_\parallel, S_\perp, S_\parallel\tilde{H}^\parallel$ and $S_\perp\tilde{H}^\perp$ are defined to recover first-order variations in x_2 using the decomposition of the local surface element into

$$A = \|\boldsymbol{e}_\theta \times \boldsymbol{e}_\phi\| = |(\boldsymbol{e}_\theta \times \boldsymbol{e}_\phi)\cdot\boldsymbol{N}| + (\|\boldsymbol{e}_\theta \times \boldsymbol{e}_\phi\| - |(\boldsymbol{e}_\theta \times \boldsymbol{e}_\phi)\cdot\boldsymbol{N}|) =: A_\parallel + A_\perp, \tag{F10}$$

where $\boldsymbol{e}_a := \partial_a \boldsymbol{r}$ for $a = \theta, \phi$, and $\boldsymbol{e}_v := \partial_v \boldsymbol{r}(u, v)$ are the tangential vectors and $\boldsymbol{N} = (0, 0, 1)$ is a constant vector chosen along the axisymmetric axis. Then for any local

https://doi.org/10.1017/jfm.2024.1200 Published online by Cambridge University Press

geometric quantity $X(u, v)$, we split the variation of the surface-averaged geometric quantity into

$$\delta(S\tilde{X}) = \delta(S_{\parallel}\tilde{X}^{\parallel}) + \delta(S_{\perp}\tilde{X}^{\perp}), \tag{F11}$$

such that we can focus on the variation $\delta(S_{\parallel}\tilde{X}^{\parallel})$, and $\delta(S_{\perp}\tilde{X}^{\perp})$ follows from (F9). The variation of $S_{\parallel}\tilde{X}^{\parallel}$ reads

$$\delta(S_{\parallel}\tilde{X}^{\parallel}) = \int_{\mathcal{U}} \delta(XA_{\parallel}) = \int_{\mathcal{U}} \delta(X|(\boldsymbol{e}_\theta \times \boldsymbol{e}_\phi)\cdot \boldsymbol{N}|). \tag{F12}$$

We get rid of the absolute value by remarking that the perturbations along harmonics Y_0 and Y_2 are symmetric with respect to the equatorial plane of the droplet. We split $\mathcal{U}$ into two hemispheres using the half-unit sphere mapping $\frac{1}{2}\mathcal{U} = (0, \pi/2) \times (0, 2\pi)$ where $(\boldsymbol{e}_\theta \times \boldsymbol{e}_\phi)\cdot \boldsymbol{N} > 0$ and perform a change of variables leading to

$$\begin{aligned}\delta(S_{\parallel}\tilde{X}^{\parallel}) &= \int_{\frac{1}{2}\mathcal{U}} \delta(X(\boldsymbol{e}_\theta \times \boldsymbol{e}_\phi)\cdot \boldsymbol{N}) - \int_{\mathcal{U}\setminus\frac{1}{2}\mathcal{U}} \delta(X(\boldsymbol{e}_\theta \times \boldsymbol{e}_\phi)\cdot \boldsymbol{N}) \\ &= 2\int_{\frac{1}{2}\mathcal{U}} \delta(X(\boldsymbol{e}_\theta \times \boldsymbol{e}_\phi))\cdot \boldsymbol{N}.\end{aligned} \tag{F13}$$

Then, the variation is decomposed following

$$\delta(S_{\parallel}\tilde{X}^{\parallel}) = 2\int_{\frac{1}{2}\mathcal{U}} \delta(XA)(\boldsymbol{n}\cdot \boldsymbol{N}) + 2\int_{\frac{1}{2}\mathcal{U}} X_0A_0\delta\boldsymbol{n}\cdot \boldsymbol{N}, \tag{F14}$$

with $A_0\delta\boldsymbol{n} = \delta(\boldsymbol{e}_\theta \times \boldsymbol{e}_\phi) - \boldsymbol{n}\delta A$. The first-order variation in x_2 is non-trivial here, and we retain only the first-order terms in ψ for $\delta(HA)$ and δA in (F3). Only the first-order variation of $\delta(\boldsymbol{e}_\theta \times \boldsymbol{e}_\phi)$ is still undetermined. For the first-order deformation $\psi = x_2Y_2 + o(x_2)$, it yields

$$\begin{aligned}\delta(\boldsymbol{e}_\theta \times \boldsymbol{e}_\phi) &= \partial_\theta \boldsymbol{r} \times \partial_\phi \boldsymbol{r} - \partial_\theta \boldsymbol{r}_0 \times \partial_\phi \boldsymbol{r}_0 \\ &= x_2R_0Y_2(\partial_\theta \boldsymbol{n} \times \partial_\phi \boldsymbol{n}) + x_2R_0(\partial_\theta Y_2)(\boldsymbol{n} \times \partial_\phi \boldsymbol{n}) \\ &\quad + R_0x_2Y_2(\partial_\theta \boldsymbol{n} \times \partial_\phi \boldsymbol{n}) + o(x_2^2).\end{aligned} \tag{F15}$$

For the sphere, we recall that

$$\left.\begin{array}{lll}\partial_\theta \boldsymbol{n} = R_0^{-1}\boldsymbol{e}_\theta, & \partial_\phi \boldsymbol{n} = R_0^{-1}\boldsymbol{e}_\phi, & \boldsymbol{e}_\theta \times \boldsymbol{e}_\phi = A_0\boldsymbol{n}, \\ A_0 = R_0^2\sin\theta, & \boldsymbol{N}\cdot\boldsymbol{n} = \cos\theta, & \boldsymbol{N}\cdot\boldsymbol{e}_\theta = -R_0\sin\theta.\end{array}\right\} \tag{F16}$$

The first-order variation $\delta(\boldsymbol{e}_\theta \times \boldsymbol{e}_\phi)$ then reads

$$\begin{aligned}\delta(\boldsymbol{e}_\theta \times \boldsymbol{e}_\phi) &= x_2R_0^{-1}Y_2(\boldsymbol{e}_\theta \times \boldsymbol{e}_\phi) + x_2(\partial_\theta Y_2)(\boldsymbol{n} \times \boldsymbol{e}_\phi) + R_0^{-1}x_2Y_2(\boldsymbol{e}_\theta \times \boldsymbol{e}_\phi) + o(x_2^2) \\ &= x_2R_0^{-1}Y_2A_0\boldsymbol{n} - x_2(\partial_\theta Y_2)A_0R_0^{-2}\boldsymbol{e}_\theta + R_0^{-1}x_2Y_2A_0\boldsymbol{n} + o(x_2^2) \\ &= 2x_2R_0^{-1}Y_2A_0\boldsymbol{n} - x_2(\partial_\theta Y_2)\boldsymbol{e}_\theta + o(x_2^2).\end{aligned} \tag{F17}$$

https://doi.org/10.1017/jfm.2024.1200 Published online by Cambridge University Press

Now, taking $X = 1$ in (F14) gives

$$\begin{aligned}\delta S_{\|} &= 2\int_{\frac{1}{2}\mathcal{U}} \delta(\boldsymbol{e}_u \times \boldsymbol{e}_v)\cdot\boldsymbol{N}\\ &= 2\int_{\frac{1}{2}\mathcal{U}} 2x_2R_0^{-1}Y_2A_0(\boldsymbol{n}\cdot\boldsymbol{N}) - x_2A_0R_0^{-2}(\partial_\theta Y_2)(\boldsymbol{e}_\theta\cdot\boldsymbol{N}) + o(x_2^2)\\ &= 4x_2R_0\int_{\frac{1}{2}\mathcal{U}} Y_2\sin\theta\cos\theta + 2x_2R_0\int_{\frac{1}{2}\mathcal{U}}(\partial_\theta Y_2)\sin^2\theta + o(x_2^2)\\ &= 4x_2R_0\frac{\sqrt{5\pi}}{8} + 2x_2R_0\left(-\frac{3\sqrt{5\pi}}{4}\right) + o(x_2^2)\\ &= -x_2R_0\sqrt{5\pi} + o(x_2^2).\end{aligned} \tag{F18}$$

For $X = H$, there is an extra term in the first-order variation $\delta(HA) = (G_0 - \frac{1}{2}\Delta)\psi A_0$ (Capovilla *et al.* 2003) which has been nullified in (F3) as the inclusion is closed. Here, it is taken into account as we integrate twice over a half-inclusion. It yields

$$\begin{aligned}\delta S_{\|}\tilde{H}^{\|} &= 2\int_{\frac{1}{2}\mathcal{U}}\delta(HA)(\boldsymbol{n}\cdot\boldsymbol{N}) + 2\int_{\frac{1}{2}\mathcal{U}} H_0(\delta(\boldsymbol{e}_\theta\times\boldsymbol{e}_\phi) - \boldsymbol{n}\delta A)\cdot\boldsymbol{N},\\ &= 2\int_{\frac{1}{2}\mathcal{U}}(G_0 - 2H_0^2)\psi A_0(\boldsymbol{n}\cdot\boldsymbol{N}) + \int_{\frac{1}{2}\mathcal{U}}\Delta\psi A_0(\boldsymbol{n}\cdot\boldsymbol{N}) + 2\int_{\frac{1}{2}\mathcal{U}} H_0\delta(\boldsymbol{e}_\theta\times\boldsymbol{e}_\phi)\cdot\boldsymbol{N},\\ &= -2x_2\int_{\frac{1}{2}\mathcal{U}} Y_2\sin\theta\cos\theta + -x_2\int_{\frac{1}{2}\mathcal{U}}(\Delta_{\mathbb{S}^2}Y_2)\sin\theta\cos\theta + 2R_0^{-1}\int_{\frac{1}{2}\mathcal{U}}\delta(\boldsymbol{e}_\theta\times\boldsymbol{e}_\phi)\cdot\boldsymbol{N},\\ &= -x_2\frac{1}{2}\sqrt{5\pi}.\end{aligned} \tag{F19}$$

Replacing x_2 with its expression in χ and S_0 yields geometric relations (4.26).

Appendix G. Weights and quadrature points of the bi-disperse quadrature

The bi-disperse closure for $n_1, n_2, (S_0)_1, (S_0)_2$ in terms of the moment in size only $M_k = M^{\xi}_{k,0,0}$ with $k = 0, 1/2, 1, 3/2$ is obtained by solving the truncated moment problem with Mathematica (Wolfram Research 2023) and reads

$$n_i = \frac{1}{2}\left(M_0 + (-1)^{i+1}\frac{3M_0M_1M_{1/2} - 2M_{1/2}^3 - M_0^2M_{3/2}}{\sqrt{\Delta}}\right), \tag{G1a}$$

$$\begin{aligned}(S_0)_i = (2(M_{1/2}^2 - M_0M_1)^2)^{-1}&(M_0^2M_{3/2}^2 - M_1^2M_{1/2}^2 + 2(M_0M_1^3 + M_{1/2}^3M_{3/2})\\ &- 4M_0M_{1/2}M_1M_{3/2} + (-1)^{i+1}(M_0M_{3/2} - M_1M_{1/2})\sqrt{\Delta}),\end{aligned} \tag{G1b}$$

with

$$\Delta = 4M_0M_1^3 - 3M_1^2M_{1/2}^2 - 6M_0M_{1/2}M_1M_{3/2} + 4M_{1/2}^3M_{3/2} + M_0^2M_{3/2}^2. \tag{G1c}$$

It can be written with the geometric variables using either relations (3.12), (4.8)–(4.9) or (4.27)–(4.28). Mathematica also shows that these relations yield positive values of n_i and

https://doi.org/10.1017/jfm.2024.1200 Published online by Cambridge University Press

$(S_0)_i$ provided that the moments M_k are positive and

$$M_{1/2}M_{3/2} - M_1^2 > 0, \quad M_0 M_1 - M_{1/2}^2 > 0. \tag{G2a,b}$$

These last two conditions ensure the positivity of Hankel matrices involved in the realisability conditions of the Hausdorff truncated moment problem (Schmüdgen 2017).

Appendix H. Hamilton's SAP for the polydisperse spray of oscillating droplets

This model is built on the basis of the two-scale model of § 2 where additional energies are added to take into account capillarity at the small scale along with the internal flow of the droplets. We recall the Lagrangian given in (4.36) for the two-scale mixture

$$\begin{aligned}\mathcal{L} = {} & \mathcal{L}_1(\alpha_1, m_1, \boldsymbol{u}) + \mathcal{L}_2(\alpha_2, m_2, \boldsymbol{u}) + \mathcal{L}_1^d(m_1^d, \rho_1^d, \boldsymbol{u}) \\ & + \mathcal{L}_1^{vib}(n_1, (S_0)_1, \chi_1, \dot{\chi}_1) + \mathcal{L}_2^{vib}(n_2, (S_0)_2, \chi_2, \dot{\chi}_1),\end{aligned} \tag{H1}$$

where $\mathcal{L}_i^{vib} = \frac{1}{2}\nu n_i (S_0)_i^{5/2}\chi_i^2 - \sigma n_i (S_0)_i - \frac{1}{2}\gamma n_i (S_0)_i \chi_i^2$. We define the action $\mathcal{A}$ associated to the Lagrangian similarly to that of Appendix B. In the same way as previous models, α_1 is a free variable in the minimisation process, while effective densities m_k are conserved, ρ_1^d is advected. For the additional variables, the number densities of droplets n_i are conserved, the surfaces $(S_0)_i$ are advected, χ_i are free variables describing the oscillatory motion of the droplets and $\dot{\chi}_i$ are linked to time derivatives of χ_i with $D_t\chi_i = \dot{\chi}_i$. This last constraint translates in terms of variations

$$\delta(\dot{\chi}_i) = \delta(D_t\chi_i) = \partial_t(\delta\chi_i) + \boldsymbol{u}\cdot\boldsymbol{\nabla}(\delta\chi_i) + \delta\boldsymbol{u}\cdot\boldsymbol{\nabla}\chi_i. \tag{H2}$$

Denoting $K_{\dot{\chi}_i} = \partial_{\dot{\chi}_i}\mathcal{L}_i^{vib}$ and $\boldsymbol{u} = \partial_{\boldsymbol{u}}\mathcal{L}$, we decompose then the variation of the action according to each dependency

$$\delta\mathcal{A}_{\alpha_1} = \int_\Omega \partial_{\alpha_1}\mathcal{L}_1\delta\alpha_1, \tag{H3}$$

$$\delta\mathcal{A}_{\alpha_2} = \int_\Omega \partial_{\alpha_2}\mathcal{L}_2\delta\alpha_2 = -\int_\Omega \alpha_1^d\boldsymbol{\nabla}(\partial_{\alpha_2}\mathcal{L}_2)\cdot\boldsymbol{\eta} - \int_\Omega \partial_{\alpha_2}\mathcal{L}_2\delta\alpha_1, \tag{H4}$$

$$\delta\mathcal{A}_{m_k} = \int_\Omega \partial_{m_k}\mathcal{L}_k\delta m_k = \int_\Omega m_k\boldsymbol{\nabla}(\partial_{m_k}\mathcal{L}_k)\cdot\boldsymbol{\eta}, \tag{H5}$$

$$\delta\mathcal{A}_{\rho_1^d} = \int_\Omega -\partial_{\rho_1^d}(\mathcal{L}_1^d + \mathcal{L}_1^{vib} + \mathcal{L}_2^{vib})\boldsymbol{\nabla}\rho_1^d\cdot\boldsymbol{\eta}, \tag{H6}$$

$$\delta\mathcal{A}_{(S_0)_i} = \int_\Omega -\partial_{(S_0)_i}\mathcal{L}_i^{vib}\boldsymbol{\nabla}(S_0)_i\cdot\boldsymbol{\eta}, \tag{H7}$$

$$\delta\mathcal{A}_{n_i} = \int_\Omega \partial_{n_i}\mathcal{L}_i^{vib}\delta n_i = \int_\Omega n_i\boldsymbol{\nabla}(\partial_{n_i}\mathcal{L}_i^{vib})\cdot\boldsymbol{\eta}, \tag{H8}$$

https://doi.org/10.1017/jfm.2024.1200 Published online by Cambridge University Press

$$\delta\mathcal{A}_{\chi_i} = \int_\Omega \partial_{\chi_i}\mathcal{L}_i^{vib}\delta\chi_i, \tag{H9}$$

$$\delta\mathcal{A}_{\dot\chi_i} = \int_\Omega K_{\dot\chi_i}\delta\dot\chi_i = \int_\Omega K_{\dot\chi_i}(\partial_t(\delta\chi_i) + \boldsymbol{u}\cdot\boldsymbol{\nabla}(\delta\chi_i) + \delta\boldsymbol{u}\cdot\boldsymbol{\nabla}\chi_i), \tag{H10}$$

$$= -\int_\Omega (\partial_t K_{\dot\chi_i} + \boldsymbol{\nabla}\cdot(K_{\dot\chi_i}\boldsymbol{u}))\delta\chi_i \tag{H11}$$

$$-\int_\Omega (\partial_t(K_{\dot\chi_i}\boldsymbol{\nabla}\chi_i) + \boldsymbol{\nabla}\cdot((K_{\dot\chi_i}\boldsymbol{\nabla}\chi_i)\boldsymbol{u}) + K_{\dot\chi_i}\boldsymbol{\nabla}\chi_i\cdot\boldsymbol{\nabla}\boldsymbol{u})\cdot\boldsymbol{\eta}, \tag{H12}$$

$$\delta\mathcal{A}_{\boldsymbol{u}} = \int_\Omega -(\partial_t\boldsymbol{K} + \boldsymbol{\nabla}\cdot(\boldsymbol{K}\otimes\boldsymbol{u}) + \boldsymbol{K}\cdot\boldsymbol{\nabla}\boldsymbol{u})\cdot\boldsymbol{\eta}. \tag{H13}$$

We denote $\mathcal{L}_k^* = m_k\partial_{m_k}\mathcal{L}_k - \mathcal{L}_k$, $\mathcal{L}_i^{vib,*} = n_i\partial_{n_i}\mathcal{L}_i^{vib} - \mathcal{L}_i^{vib}$ and $\mathcal{L}^* = \mathcal{L}_1^* + \mathcal{L}_2^* + \mathcal{L}_1^{d,*}$ such that the variation of the action related to the mixture Lagrangian reads

$$\delta\mathcal{A} = \int \boldsymbol{A}_{\boldsymbol{\eta}}\cdot\boldsymbol{\eta} + \boldsymbol{A}_{\alpha_1}\delta\alpha_1 + \boldsymbol{A}_{\chi_1}\delta\chi_1 + \boldsymbol{A}_{\chi_2}\delta\chi_2, \tag{H14}$$

with

$$\left.\begin{gathered}\boldsymbol{A}_{\alpha_1} = \partial_{\alpha_1}\mathcal{L}_1 - \partial_{\alpha_2}\mathcal{L}_2,\\ \boldsymbol{A}_{\chi_i} = \partial_{\chi_i}\mathcal{L}_k^{vib} - \partial_t K_{\dot\chi_i} - \boldsymbol{\nabla}\cdot(K_{\dot\chi_i}\boldsymbol{u}),\\ \boldsymbol{A}_{\boldsymbol{\eta}} = -(\partial_t\boldsymbol{K} + \boldsymbol{\nabla}\cdot(\boldsymbol{K}\otimes\boldsymbol{u}) - \boldsymbol{\nabla}(\mathcal{L}^* - \alpha_1^d\partial_{\alpha_2}\mathcal{L}_2) - \boldsymbol{A}_{\alpha_1}\boldsymbol{\nabla}\alpha_1 - \boldsymbol{A}_{\chi_1}\boldsymbol{\nabla}\chi_1 - \boldsymbol{A}_{\chi_2}\boldsymbol{\nabla}\chi_2)\end{gathered}\right\} \tag{H15}$$

and $\mathcal{L}_i^{vib,*} := n_i\partial_{n_i}\mathcal{L}_i^{vib} - \mathcal{L}_i^{vib}$. Nullifying the variations gives the following system:

$$\left.\begin{gathered}\partial_t\boldsymbol{K} + \boldsymbol{\nabla}\cdot(\boldsymbol{K}\otimes\boldsymbol{u}) - \boldsymbol{\nabla}(\mathcal{L}^* - \alpha_1^d\partial_{\alpha_2}\mathcal{L}_2) = 0,\\ \partial_{\chi_1}\mathcal{L}_1^{vib} - \partial_t K_{\dot\chi_1} - \boldsymbol{\nabla}\cdot(K_{\dot\chi_1}\boldsymbol{u}) = 0,\\ \partial_{\chi_2}\mathcal{L}_2^{vib} - \partial_t K_{\dot\chi_2} - \boldsymbol{\nabla}\cdot(K_{\dot\chi_2}\boldsymbol{u}) = 0,\\ \partial_{\alpha_1}\mathcal{L}_1 - \partial_{\alpha_2}\mathcal{L}_2 = 0.\end{gathered}\right\} \tag{H16}$$

Evaluating the derivatives of the Lagrangian as defined in (4.37) yields

$$\left.\begin{gathered}\boldsymbol{K}_{\boldsymbol{u}} = \partial_{\boldsymbol{u}}\mathcal{L} = \rho\boldsymbol{u}, \quad \mathcal{L}^* = -\alpha_1 p_1 - \alpha_2 p_2, \quad \partial_{\alpha_2}\mathcal{L}_2 = p_2, \quad \partial_{\alpha_1}\mathcal{L}_1 = p_1,\\ \partial_{\chi_i}\mathcal{L}_i^{vib} = -\gamma n_i(S_0)_i\chi_i, \quad K_{\dot\chi_i} = \partial_{\dot\chi_i}\mathcal{L}_i^{vib} = \nu n_i(S_0)_i^{5/2}\dot\chi_i.\end{gathered}\right\} \tag{H17}$$

Finally, with the constraints and the relation $D_t\chi_i = \dot\chi_i$, we write the final system in its conservative form

$$\left.\begin{gathered}\partial_t m_k + \boldsymbol{\nabla}\cdot(m_k\boldsymbol{u}) = 0, \quad k = 1, 2, 1^d,\\ \partial_t n_i + \boldsymbol{\nabla}\cdot(n_i\boldsymbol{u}) = 0, \quad i = 1, 2,\\ \partial_t(n_i(S_0)_i) + \boldsymbol{\nabla}\cdot(n_i(S_0)_i\boldsymbol{u}) = 0, \quad i = 1, 2,\\ \partial_t(n_i\dot\chi_i) + \boldsymbol{\nabla}\cdot(n_i\dot\chi_i\boldsymbol{u}) = -\omega_i^2 n_i\chi_i, \quad i = 1, 2,\\ \partial_t(n_i\chi_i) + \boldsymbol{\nabla}\cdot(n_i\chi_i\boldsymbol{u}) = n_i\dot\chi_i, \quad i = 1, 2,\\ \partial_t(\rho\boldsymbol{u}) + \boldsymbol{\nabla}\cdot(\rho\boldsymbol{u}\otimes\boldsymbol{u} + p\boldsymbol{I}) = 0,\end{gathered}\right\} \tag{H18}$$

where $p := p_1 = p_2$ and $\omega_i^2 = \gamma/\nu(S_0)_i^{-3/2}$.

https://doi.org/10.1017/jfm.2024.1200 Published online by Cambridge University Press

Appendix I. The monodisperse case

Even though the polydispersion is a key feature of our model, we can also consider a monodisperse model to obtain a minimal model. In this case, only four geometric quantities are required, two related to statics and two related to dynamics. Compatibility with § 2 leads us to consider $(\Sigma\langle G\rangle, \alpha_1^d, (\Delta\Sigma_\perp), (\Delta_t\Sigma_\perp))$ or, equivalently, $(n_1^d, \alpha_1^d, (\Delta\Sigma_\perp), (\Delta_t\Sigma_\perp))$. We then obtain the following quadrature:

$$\left.\begin{gathered} n(\boldsymbol{x}, t, \hat{S}_0, \hat{\chi}, \hat{\dot{\chi}}) = n_1^d \delta(\hat{S}_0 - S_0)\delta(\hat{\chi} - \chi)\delta(\hat{\dot{\chi}} - \dot{\chi}), \quad S_0 = \frac{(6\sqrt{\pi}\alpha_1^d)^{2/3}}{(n_1^d)^{2/3}}, \\ \chi = 2\sqrt{\frac{2}{5}}\frac{(\Delta\Sigma_\perp)}{(n_1^d)^{1/3}(6\sqrt{\pi}\alpha_1^d)^{2/3}}, \quad \dot{\chi} = 2\sqrt{\frac{2}{5}}\frac{(\Delta_t\Sigma_\perp)}{(n_1^d)^{1/3}(6\sqrt{\pi}\alpha_1^d)^{2/3}}. \end{gathered}\right\} \tag{I1}$$

All other geometric quantities can then be reconstructed through moments of n. The minimisation of the Lagrangian is similar to the polydisperse one, and, without adding dissipative source terms, we obtain the following set of equations

$$\left.\begin{gathered} \partial_t m_k + \boldsymbol{\nabla}\cdot(m_k\boldsymbol{u}) = 0, \quad k = 1, 2, 1^d, \\ \partial_t n_1^d + \boldsymbol{\nabla}\cdot(n_1^d\boldsymbol{u}) = 0, \\ \partial_t(n_1^d(S_0)) + \boldsymbol{\nabla}\cdot(n_1^d(S_0)\boldsymbol{u}) = 0, \\ \partial_t(n_1^d\dot{\chi}) + \boldsymbol{\nabla}\cdot(n_1^d\dot{\chi}\boldsymbol{u}) = -\omega^2 n_1^d\chi, \\ \partial_t(n_1^d\chi) + \boldsymbol{\nabla}\cdot(n_1^d\chi\boldsymbol{u}) = n_1^d\dot{\chi}, \\ \partial_t(\rho\boldsymbol{u}) + \boldsymbol{\nabla}\cdot(\rho\boldsymbol{u}\otimes\boldsymbol{u} + p\boldsymbol{I}) = 0, \end{gathered}\right\} \tag{I2}$$

with $p := p_1 = p_2$ where $\omega^2 = \tilde{\omega}^2(S_0)^{-3/2}$ and $\beta = 40\pi\nu_{vis}/S_0$. We can then provide the dynamics of other geometric quantities such as the interface area density $\Sigma = M^\xi_{1,0,0} + M^\xi_{1,2,0}$,

$$\partial_t\Sigma + \boldsymbol{\nabla}\cdot(\Sigma\boldsymbol{u}) = \partial_t(n_1^d(S_0)\chi^2) + \boldsymbol{\nabla}\cdot(n_1^d(S_0)\chi^2\boldsymbol{u}) = n_1^d(S_0)D_t(\chi^2) = 2n_1^d(S_0)\chi\dot{\chi}. \tag{I3}$$

Replacing with geometric variables leads to

$$\partial_t\Sigma + \boldsymbol{\nabla}\cdot(\Sigma\boldsymbol{u}) = \frac{16}{5}\frac{(\Delta\Sigma_\perp)(\Delta_t\Sigma_\perp)}{(n_1^d)^{1/3}(6\sqrt{\pi}\alpha_1^d)^{2/3}}. \tag{I4}$$

We remark that we cannot get rid of the oriented surface area density terms in all terms of the evolution equation of Σ. Moreover, no parameter of the physics is present.

References

Amsden, A.A., O'Rourke, P.J. & Butler, T.D. 1989 KIVA-II: a computer program for chemically reactive flows with sprays. *Tech. Rep.* LA-11560-MS, 6228444. Los Alamos National Laboratory.

Anez, J., Ahmed, A., Hecht, N., Duret, B., Reveillon, J. & Demoulin, F.-X. 2019 Eulerian–Lagrangian spray atomization model coupled with interface capturing method for diesel injectors. *Intl J. Multiphase Flow* **113**, 325–342.

Baer, M.R. & Nunziato, J.W. 1986 A two-phase mixture theory for the deflagration-to-detonation transition (DDT) in reactive granular materials. *Intl J. Multiphase Flow* **12** (6), 861–889.

Bedford, A. 1985 *Hamilton's Principle in Continuum Mechanics*. Pitman Publishing.

Berdichevsky, V. 2009 *Variational Principles of Continuum Mechanics: I. Fundamentals*, Interaction of Mechanics and Mathematics, vol. 5. Springer.

Capovilla, R., Guven, J. & Santiago, J.A. 2003 Deformations of the geometry of lipid vesicles. *J. Phys.* A **36** (23), 6281–6295.

https://doi.org/10.1017/jfm.2024.1200 Published online by Cambridge University Press

CARO, F., COQUEL, F., JAMET, D. & KOKH, S. 2005 DINMOD: a diffuse interface model for two-phase flows modelling. In *IRMA Lectures in Mathematics and Theoretical Physics*, pp. 209–237. EMS Press.

CHANTEPERDRIX, G., VILLEDIEU, P. & VILA, J.-P. 2002 A compressible model for separated two-phase flows computations. In *FEDSM2002*, vol. 1, pp. 809–816. ASME.

CORDESSE, P. 2020 Contribution to the study of combustion instabilities in cryotechnic rocket engines: coupling diffuse interface models with kinetic-based moment methods for primary atomization simulations. PhD thesis, Université Paris-Saclay.

CORDESSE, P., DI BATTISTA, R., CHEVALIER, Q., MATUSZEWSKI, L., MÉNARD, T., KOKH, S. & MASSOT, M. 2020*a* A diffuse interface approach for disperse two-phase flows involving dual-scale kinematics of droplet deformation based on geometrical variables. *ESAIM: Proc. Surv.* **69**, 24–46.

CORDESSE, P., REMIGI, A., DURET, B., MURRONE, A., MÉNARD, T., DEMOULIN, F.-X. & MASSOT, M. 2020*b* Validation strategy of reduced-order two-fluid flow models based on a hierarchy of direct numerical simulations. *Flow Turbul. Combust.* **105** (4), 1381–1411.

DESERNO, M. 2015 Fluid lipid membranes: from differential geometry to curvature stresses. *Chem. Phys. Lipids* **185**, 11–45.

DEVASSY, B.M., HABCHI, C. & DANIEL, E. 2015 Atomization modelling of liquid jets using a two-surface density approach. *Atomiz. Sprays* **25** (1), 47–80.

DREW, D.A. 1983 Mathematical modeling of two-phase flow. *Annu. Rev. Fluid Mech.* **15**, 261–291.

DREW, D.A. 1990 Evolution of geometric statistics. *SIAM J. Appl. Math.* **50** (3), 649–666.

DREW, D.A. & PASSMAN, S.L. 1999 *Theory of Multicomponent Fluids*, Applied Mathematical Sciences, vol. 135. Springer.

DRUI, F., LARAT, A., KOKH, S. & MASSOT, M. 2019 Small-scale kinematics of two-phase flows: identifying relaxation processes in separated- and disperse-phase flow models. *J. Fluid Mech.* **876**, 326–355.

DUMOUCHEL, C., BLAISOT, J.-B., BOUCHE, E., MÉNARD, T. & VU, T.-T. 2015 Multi-scale analysis of atomizing liquid ligaments. *Intl J. Multiphase Flow* **73**, 251–263.

ESSADKI, M., DE CHAISEMARTIN, S., LAURENT, F. & MASSOT, M. 2018 High order moment model for polydisperse evaporating sprays towards interfacial geometry description. *SIAM J. Appl. Maths* **78** (4), 2003–2027.

ESSADKI, M., DE CHAISEMARTIN, S., MASSOT, M., LAURENT, F., LARAT, A. & JAY, S. 2016 Adaptive mesh refinement and high order geometrical moment method for the simulation of polydisperse evaporating sprays. *Oil Gas Sci. Technol.* **71** (5), 01395317.

ESSADKI, M., DRUI, F., DE CHAISEMARTIN, S., LARAT, A., MÉNARD, T. & MASSOT, M. 2019 Statistical modeling of the gas–liquid interface using geometrical variables: toward a unified description of the disperse and separated phase flows. *Intl J. Multiphase Flow* **120**, 103084.

ESTIVALEZES, J.-L., *et al.* 2022 A phase inversion benchmark for multiscale multiphase flows. *J. Comput. Phys.* **450**, 110810.

FIORINA, B., *et al.* 2016 Modeling challenges in computing aeronautical combustion chambers. *Aerosp. Lab J.* **5** (11), 1–19.

FOX, R.O. & MARCHISIO, D.L. (Eds) 2007 *Multiphase Reacting Flows: Modelling and Simulation*, Courses and Lectures, no. 492. Springer.

GAILLARD, P. 2015 Interfaces diffuses et flammes transcritiques LOX/H2. PhD thesis, Universite Pierre et Marie Curie.

GAVRILYUK, S. 2020 'Uncertainty' principle in two fluid-mechanics. *ESAIM: Proc. Surv.* **69**, 47–55.

GAVRILYUK, S. & GOUIN, H. 1999 A new form of governing equations of fluids arising from Hamilton's principle. *Intl J. Engng Sci.* **37** (12), 1495–1520.

GAVRILYUK, S., GOUIN, H. & PEREPECHKO, Y.V. 1998 Hyperbolic models of homogeneous two-fluid mixtures. *Meccanica* **33** (2), 161–175.

GAVRILYUK, S. & SAUREL, R. 2002 Mathematical and numerical modeling of two-phase compressible flows with micro-inertia. *J. Comput. Phys.* **175** (1), 326–360.

GODLEWSKI, E. & RAVIART, P.-A. 1991 *Hyperbolic Systems Of Conservation Laws*. Springer.

GOLDMAN, R. 2005 Curvature formulas for implicit curves and surfaces. *Comput. Aided Geom. Des.* **22** (7), 632–658.

GOUIN, H. 2020 *Introduction to Mathematical Methods of Analytical Mechanics*. ISTE Press/Elsevier.

GOUIN, H. & GAVRILYUK, S. 1999 Hamilton's principle and Rankine–Hugoniot conditions for general motions of mixtures. *Meccanica* **34** (1), 39–47.

HERIVEL, J.W. 1955 The derivation of the equations of motion of an ideal fluid by Hamilton's principle. *Math. Proc. Camb. Phil. Soc.* **51** (2), 344–349.

ISHII, M. & HIBIKI, T. 1975 *Thermo-fluid Dynamic Theory of Two-phase Flow*. Eyrolles.

JABIN, P.-E. 2002 Various levels of models for aerosols. *Math. Models Meth. Appl. Sci.* **12** (07), 903–919.

https://doi.org/10.1017/jfm.2024.1200 Published online by Cambridge University Press

JAMET, D., LEBAIGUE, O., MOREL, C. & ARCEN, B. 2010 Towards a multi-scale approach of two-phase flow modeling in the context of DNB modeling. *Nucl. Engng Des.* **240** (9), 2131–2138.

KAH, D., EMRE, O., TRAN, Q.H., DE CHAISEMARTIN, S., JAY, S., LAURENT, F. & MASSOT, M. 2015 High order moment method for polydisperse evaporating sprays with mesh movement: application to internal combustion engines. *Intl J. Multiphase Flow* **71**, 38–65.

KREYSZIG, E. 1991 *Differential Geometry*. Dover.

LAURENT, F. & MASSOT, M. 2001 Multi-fluid modelling of laminar polydisperse spray flames: origin, assumptions and comparison of sectional and sampling methods. *Combust. Theory Model.* **5** (4), 537–572.

LE TOUZE, C., DOREY, L.-H., RUTARD, N. & MURRONE, A. 2020 A compressible two-phase flow framework for large eddy simulations of liquid-propellant rocket engines. *Appl. Math. Model.* **84**, 265–286.

LEBAS, R., MENARD, T., BEAU, P.-A., BERLEMONT, A. & DEMOULIN, F.-X. 2009 Numerical simulation of primary break-up and atomization: DNS and modelling study. *Intl J. Multiphase Flow* **35** (3), 247–260.

LEVERMORE, C.D. 1996 Moment closure hierarchies for kinetic theories. *J. Stat. Phys.* **83** (5–6), 1021–1065.

LHUILLIER, D. 2004 Evolution of the volumetric interfacial area in two-phase mixtures. *C. R. Méc* **332** (2), 103–108.

LOISON, A., KOKH, S., PICHARD, T. & MASSOT, M. 2024 A unified two-scale gas–liquid multi-fluid model with capillarity and interface regularization through a mass transfer between scales. *Intl J. Multiphase Flow* **177**, 104857.

MARCHISIO, D.L. & FOX, R.O. 2013 *Computational Models for Polydisperse Particulate and Multiphase Systems*. Cambridge University Press.

MASSOT, M. 2007 Eulerian multi-fluid models for polydisperse evaporating sprays. In *Multiphase Reacting Flows: Modelling and Simulation* (ed. D.L. Marchisio & R.O. Fox), pp. 79–123. Springer.

MASSOT, M., KUMAR, M., GOMEZ, A. & SMOOKE, M. 1998 Counterflow spray diffusion flames of heptane: computations and experiments. In *Proceedings of the 27th Symposium International on Combustion*, pp. 1975–1983. The Combustion Institute.

MEAD, L.R. & PAPANICOLAOU, N. 1984 Maximum entropy in the problem of moments. *J. Math. Phys.* **25** (8), 2404–2417.

MOREL, C. 2015 *Mathematical Modeling of Disperse Two-Phase Flows*, Fluid Mechanics and its Applications, vol. 114. Springer.

MÉNARD, T., TANGUY, S. & BERLEMONT, A. 2007 Coupling level set/VOF/ghost fluid methods: validation and application to 3D simulation of the primary break-up of a liquid jet. *Intl J. Multiphase Flow* **33** (5), 510–524.

O'ROURKE, P.J. & AMSDEN, A.A. 1987 The tab method for numerical calculation of spray droplet breakup. In *SAE Tech. Paper* 872089.

PELANTI, M. 2022 Arbitrary-rate relaxation techniques for the numerical modeling of compressible two-phase flows with heat and mass transfer. *Intl J. Multiphase Flow* **153**, 104097.

PERIGAUD, G. & SAUREL, R. 2005 A compressible flow model with capillary effects. *J. Comput. Phys.* **209** (1), 139–178.

PERRIER, V. & GUTIÉRREZ, E. 2021 Derivation and closure of Baer and Nunziato type multiphase models by averaging a simple stochastic model. *Multiscale Model. Simul.* **19** (1), 401–439.

PILCH, M. & ERDMAN, C.A. 1987 Use of breakup time data and velocity history data to predict the maximum size of stable fragments for acceleration-induced breakup of a liquid drop. *Intl J. Multiphase Flow* **13** (6), 741–757.

PLÜMACHER, D., OBERLACK, M., WANG, Y. & SMUDA, M. 2020 On a non-linear droplet oscillation theory via the unified method. *Phys. Fluids* **32** (6), 067104.

POPE, S.B. 1988 The evolution of surface in turbulence. *Intl J. Engng Sci.* **26** (5), 445–469.

PROSPERETTI, A. 1977 Viscous effects on perturbed spherical flows. *Q. Appl. Maths* **34** (4), 339–352.

PROVIDAKIS, T., ZIMMER, L., SCOUFLAIRE, P., DUCRUIX, S. 2012 Characterization of the acoustic interactions in a two-stage multi-injection combustor fed with liquid fuel. *Trans. ASME: J. Engng Gas Turbine. Power* **134** (11), 111503.

RAVIART, P.-A. & SAINSAULIEU, L. 1995 A non-conservative hyperbolic system modeling spray dynamics. Part I. Solution of the Riemann problem. *Math. Models Meth. Appl. Sci.* **5** (3), 297–333.

RAYLEIGH, LORD 1879 VI. On the capillary phenomena of jets. *Proc. R. Soc.* **29** (196-199), 71–97.

SAKANO, Y., NAMBU, T., MIZOBUCHI, Y. & SATO, T. 2022 Evaluation of three-dimensional droplet shape for analysis of the crossflow-type atomization. *Mech. Engng J.* **9** (1), 21-00378.

SALMON, R. 1983 Practical use of Hamilton's principle. *J. Fluid Mech.* **132**, 431–444.

SAUREL, R., CHINNAYYA, A. & CARMOUZE, Q. 2017 Modelling compressible dense and dilute two-phase flows. *Phys. Fluids* **29** (6), 063301.

https://doi.org/10.1017/jfm.2024.1200 Published online by Cambridge University Press

SAUREL, R., GAVRILYUK, S. & RENAUD, F. 2003 A multiphase model with internal degrees of freedom: application to shock–bubble interaction. *J. Fluid Mech.* **495**, 283–321.
SCARDOVELLI, R. & ZALESKI, S. 1999 Direct numerical simulation of free-surface an interfacial flow. *Annu. Rev. Fluid Mech.* **31** (1), 567–603.
SCHMIDMAYER, K., PETITPAS, F., DANIEL, E., FAVRIE, N. & GAVRILYUK, S. 2017 A model and numerical method for compressible flows with capillary effects. *J. Comput. Phys.* **334**, 468–496.
SCHMÜDGEN, K. 2017 *The Moment Problem*, Graduate Texts in Mathematics, vol. 277. Springer.
SERRE, D. 2010 The structure of dissipative viscous system of conservation laws. *Physica* D*: Nonlinear Phenom.* **239** (15), 1381–1386.
SERRIN, J. 1959 Mathematical principles of classical fluid mechanics. In *Fluid Dynamics I/Strömungsmechanik I* (ed. C. Truesdell), pp. 125–263. Springer.
SHINJO, J. & UMEMURA, A. 2010 Simulation of liquid jet primary breakup: dynamics of ligament and droplet formation. *Intl J. Multiphase Flow* **36** (7), 513–532.
TOMAR, G., FUSTER, D., ZALESKI, S. & POPINET, S. 2010 Multiscale simulations of primary atomization. *Comput. Fluids* **39** (10), 1864–1874.
TRUSKINOVSKY, L. 1991 Kinks versus shocks. In *Shock Induced Transitions and Phase Structures in General Media* (ed. R. Fosdick, J.E. Dunn & M. Slemrod), The IMA Volumes in Mathematics and its Applications, vol. 52. Springer.
VALLET, A. & BORGHI, R. 1999 Modélisation eulerienne de l'atomisation d'un jet liquide. *C. R. Acad. Sci.* IIB **327** (10), 1015–1020.
VIÉ, A., LAURENT, F. & MASSOT, M. 2013 Size-velocity correlations in high order moment methods for polydisperse evaporating sprays: modeling and numerical issues. *J. Comput. Phys.* **237**, 177–210.
WILLIAMS, F.A. 1958 Spray combustion and atomization. *Phys. Fluids* **1** (6), 6.
WOLFRAM RESEARCH, INC. 2023 Mathematica, Version 13.3.

https://doi.org/10.1017/jfm.2024.1200 Published online by Cambridge University Press